Evolution of the sauropodomorph astragalus: relationships with the emergence of the sauropod bauplan and weight-bearing function, and critical appraisal of evolutionary rate estimation

Rémi Lefebvre[1,2,3*], Chloé Aubry[4], Heinrich Mallison[5], Alexandra Houssaye[4]

[1] Institut de Systématique, Évolution, Biodiversité, UMR7205, SU, MNHN, CNRS, EPHE, UA, Muséum National d'Histoire Naturelle, 45 rue Buffon, CP50, 75005 Paris, France; remi.lefebvre.mail@gmail.com, ORCiD : 0000-0003-4388-6852

[2] JURASSICA Museum, Route de Fontenais 21, 2900 Porrentruy, Switzerland

[3] Department of Geosciences, University of Fribourg, Chemin du Musée 4, 1700 Fribourg, Switzerland

[4] Mécanismes Adaptatifs et Évolution, UMR 7179, CNRS, MNHN, Muséum National d'Histoire Naturelle, 55 rue Buffon, CP55, 75005 Paris, France

[5] Palaeo3D, Rain, Germany

This is a pre-copyedited, author-produced PDF of an article accepted for publication in the Zoological Journal of the Linnean Society following peer review. The version of record (Rémi Lefebvre, Chloé Aubry, Heinrich Mallison, Alexandra Houssaye, Evolution of the sauropodomorph astragalus: relationships with the emergence of the sauropod bauplan and weight-bearing function, and critical appraisal of evolutionary rate estimation, Zoological Journal of the Linnean Society, Volume 204, Issue 4, August 2025, zlaf077, https://doi.org/10.1093/zoolinnean/zlaf077) is available online at: https://academic.oup.com/zoolinnean/article-abstract/204/4/zlaf077/8224426.

Abstract

Sauropods, the largest terrestrial animals, were a clade of quadrupedal dinosaurs nested within sauropodomorphs, whose early representatives were small bipeds. Their evolution towards gigantism was associated with acquisition of specialized features, notably the columnar limbs. However, their tarsus, mainly represented by the astragalus, received little attention despite its critical position and role in limb architecture. We aim at quantifying the 3D shape of a large sample of sauropodomorph astragali to assess how its morphology evolved through time and with the emergence of the sauropod bauplan. Acquisition of sauropod-related features was stepwise, congruently with previous results for the hindlimb zeugopod, with marked distinction and diversification of the eusauropod subclade. Size-related variations were congruent with weight-bearing constraints, with flatter distal articular surfaces and more tightly interlocked proximal ones. The subhorizontal pes organisation in eusauropods is comparable to that in elephants, suggesting a link with the evolution of an extensive foot pad in both groups. Our evolutionary rates analysis *could* appear as supporting this hypothesis. However, our randomization procedure showed that our test was highly sensitive to temporal uncertainties. Our case study therefore encourages acknowledging sensitivity in phylogenetically-informed palaeobiological analyses, to more robustly assess the degree of confidence to put on subsequent interpretations.

Additional keywords: Sauropoda; tarsus; graviportality; functional morphology; geometric morphometrics; evolutionary rates; biomechanics; phylogenetic characters

Introduction

In terrestrial tetrapods, the postcranial skeleton is one of the main structures supporting organs and handling the biomechanical constraints related to weight support and locomotion (Hildebrand 1982, Biewener 1989). Large and heavy animals are often said to be “graviportal”, a polysemic terminology generally used to qualify slowly moving and heavy taxa showing strong association between the form of their bones (among other support structures) and their efficiency in performing weight-bearing function (Gregory 1912, Osborn 1929, Coombs 1978, Hildebrand 1982, Carrano 1999, 2005, Polly 2007, Angst et al. 2016, Houssaye et al. 2016, Hutchinson 2021, Lefebvre *et al.* 2022, 2023, Bader et al. 2024; but see also Mallet et al. 2022 questioning the relevance of the terminology). Across studies using this term, some groups such as elephants and sauropods are consensually classified as graviportal, often because of their particular limb architecture (see Lefebvre et al. 2022 and Bader et al. 2024), whereas groups such as rhinoceroses (see Mallet et al. 2022) and large flightless birds (Angst et al. 2016) are also qualified as such, relying on different criteria (e.g. limb proportions, locomotor repertoire, see Carrano 1999). No matter the exact definition, most studies have focused on characterizing the condition of morphological features in weight-bearing bones. Particular attention has been paid to the mammalian tarsus, from the earliest works coining the term “graviportality” (Gregory 1912, Osborn 1929) to studies relying on more recent quantitative frameworks (Etienne et al. 2020). Concretely, heavy mammals tend to show more flattened and wider articular surface in their astragalus, the main tarsal bone in contact with the tibia. Those articular surfaces appear more proximally oriented, which participates in decreasing limb angulation (hence increasing limb straightening), thereby resulting in a more efficient position for weight bearing (Osborn 1900, Gregory 1912, Osborn 1929, Etienne et al. 2020). The evolution of tarsal morphology in relation to variation in body mass is therefore critical as this subunit is predominantly involved in weight bearing in a standing quadruped, whereas the carpus may be partly or totally relaxed from such constraint in partially to totally bipedal animals.

However, the morphological evolution of the tarsus in relation to the functional constraints related to a high body mass and/or size remained insufficiently studied in non-mammalian amniotes. This paucity of studies is particularly surprising in the case of sauropod dinosaurs, since they include the largest terrestrial animals that ever existed, with gigantic forms exceeding several dozens of meters and tons (Sander & Clauss 2008, Sander et al. 2011). Sauropods were all obligatory quadrupedal animals that convergently with elephants evolved a columnar (i.e., straight) limb architecture (Osborn 1900, Christiansen 1997, Lefebvre et al. 2022, Bader et al. 2023, 2024). Sauropods constitute a clade included within sauropodomorphs, whose early representatives were much smaller and showed a wider locomotor diversity (see Lefebvre et al 2022). Although some non-sauropodan sauropodomorph taxa reached substantially large body dimensions (Apaldetti et al. 2018, McPhee et al. 2018), they never reached the extreme gigantism seen in sauropods (e.g. Carballido et al. 2017, Apaldetti et al. 2018, Sander et al. 2011). Gigantic dimensions were probably possible because of the unique suite of morphological features found in the sauropod bauplan (Salgado et al. 1997, Wilson & Sereno, 1988, Sander et al. 2011, Rauhut et al. 2011, Lefebvre et al. 2022, 2023), that likely contributed to their post-Toarcian radiation (Allain & Aquesbi 2008, Pol et al. 2020). Retracing how sauropod bauplan-related features emerged within sauropodomorphs, including the acquisition of columnar limbs and obligate quadrupedality, is thus critical to understand how the most extreme gigantism ever found in terrestrial animals evolved within this clade.

Tarsal evolution is even more critical for this group, considering that a substantial number of sauropods were inferred to have a rather posterior centre of mass (Henderson 2006; Mallison 2011; Otero et al. 2019) implying higher pressures related to weight on the hindlimbs than on the forelimbs. However, their ankle articulation strongly differs from the mammalian condition across amniotes. Functionally, while the mammalian ankle mobility is centred mainly between the astragalus and the distal zeugopod (Polly 2007), a wider articular diversity exists within archosaurs.

In extant taxa, two archetypes exist: the crurotarsal articulation (mainly between the astragalus and calcaneum) observed in crocodilians, and the mesotarsal articulation (between the (tibio)tarsus and (tarso)metatarsals) seen in birds. Fossil species can be identified as belonging to one of them, or differ along an evolutionary continuum in between those two archetypes (Brinkman 1981; Novas, 1989, Turner & Gatesy, 2023). Developmentally, the formation of the tarsus is complex and diverse across amniotes, with multiple centres of ossification (O'Keefe et al. 2006; Blanco et al. 2020). Specifically for dinosaurs, embryological evidence suggests that the astragalus may result from a unique ossification pattern (Ossa-Fuentes et al. 2015), which means that it should not be considered as totally homologous to the mammalian talus.

In sauropodomorphs, the astragalus is the main ossified structure of the tarsus, whereas the calcaneum is very reduced, if not totally absent or unossified (Bonnan 2000, 2005, Tschopp et al. 2015a). Embedded within a mesotarsal articulation, as in other dinosaurs, the astragalus is firmly connected to the tibial distal end, so that ankle mobility occurs around the astragalar distal surface (Bonnan 2005). More distal tarsals are also found in non-sauropodan sauropodomorphs (see e.g. Cooper, 1981; Galton & Van Heerden 1998; Apaldetti et al. 2013), but not in sauropod pedes (Bonnan 2005, Tschopp et al. 2015a). It is hypothesized that such elements are truly absent or fused with metatarsals, hence giving to sauropods a unique ankle configuration, or perhaps were unossified cartilaginous elements (Bonnan 2005, Tschopp et al. 2015a, Jannel et al. 2019).

The evolutionary sequence that led to the emergence of the sauropod bauplan is thought to have occurred during a very short period of time (Allain & Aquesbi 2008; Pol et al. 2020; Lefebvre et al. 2022), in association with the key acquisition of the columnar limb architecture (see e.g. Wilson & Sereno 1998). A recent study quantitatively highlighted the drastic morphological differences in sauropod and non-sauropodan sauropodomorph limb long bones, with abrupt acquisition of sauropod-related features in the forelimb elements, and a more gradual evolution in the hindlimb bones (Lefebvre et al. 2022). The evolution of the tarsus also received attention from earlier studies partly associating its evolution to this context, with a reorientation of the astragalus in sauropods

(Cooper 1984, Bonnan 2005) resulting from the development of the ascending process towards the posterior margin of the astragalus (Wilson & Sereno 1998, Bonnan 2005). This configuration is interpreted to result in a more horizontal orientation of metatarsals, that could have maintained powerful plantarflexion capacities (Bonnan 2005, but see also Jannel et al. 2019). This functional hypothesis resulting from shape variation in the sauropodomorph astragalus was, however, poorly examined quantitatively.

Given this context, it appears critical to retrace how astragalar morphology evolved through time in association with the emergence of the sauropod bauplan and gigantism. Relying on 3D geometric morphometrics (3DGM; Mitteroecker & Gunz 2009) and surface sliding semilandmarks (Gunz & Mitteroecker 2013), we quantify the whole shape variation of a large sample of sauropodomorphs. We highlight how morphology is linked to gigantism, by examining the significance of the relationship between astragalar shape and size (i.e., allometry, Klingenberg 2016), taking acquisition of the specific columnar limb architecture into account. Considering that a differential trend was detected between non-columnar-limbed sauropodomorphs and columnar-limbed sauropods for the hindlimb zeugopod (Lefebvre et al. 2022), we may expect to find a similar pattern with the astragalus. Next, we inferred how morphological variation occurred through time along the evolutionary history in the group. To do so, we estimated the rates of morphological evolution of the sauropodmorph astragalus in a phylogenetically-informed context (Castiglione et al. 2018), with particular attention to sensitivity related to stratigraphic uncertainty. Considering that emergence of sauropod-related traits occurred over a short period of time and was associated to a faunal turnover (Allain & Aquesbi 2008; Pol et al. 2020), and that size-related morphological variation may be different between sauropods and other sauropodomorphs (Lefebvre et al. 2022), we may expect that the emergence and radiation of the sauropod bauplan is associated to a shift in evolutionary rates.

Material and Methods

Sampling and digitization

We gathered a sample of 45 astragali (Table S1) representing the locomotor diversity found within sauropodomorphs (see phylogenetic framework). Specimens were digitized into 3D models using either (1) a surface scanner Artec EVA and the software Artec Studio 12 (Artec 3D 2018), (2) Computed tomography scan data and (3) photogrammetry and the software Agisoft Photoscan/Metashape Pro (Agisoft LLC 2018) or Reality Capture (Capturing Reality s.r.o. 2018), following recommendations of Mallison and Wings (2014) and Fau et al. (2016). In order to facilitate the analyses, the 3D models were decimated using the software Meshlab (Cignoni et al. 2008) or GOMinspect (GOM GmbH 2018) when they were above the limit of 500,000 faces. The left bones were symmetrized arbitrarily on the right side for the purpose of the analysis using the same software. Because 3DGM analyses are sensitive to taphonomic deformations and incompletenesses (Hedrick & Dodson, 2013, Lefebvre et al. 2020) we graded every specimen for those two potential noise sources following the protocol established by Lefebvre et al. (2022), resulting in discarding 9 specimens (see Table S1).

Phylogenetic framework

Following the approach in Lefebvre et al. (2022), our sampling strategy is focused in providing a representative selection of morphofunctional groups known within sauropodomorphs (Figure 1). Among the non-sauropodan sauropodomorphs paraphyletic grade, this includes non-sauropodiforms sauropodmorphs (in green), majoritarily seen as obligate to habitually bipedal, and non-sauropodomorph sauropodiforms (in orange) that are traditionnally seen as showing successive innovations indicative of likely quadrupedal habits (see Lefebvre et al. 2022). Our sample also comprises a large part of sauropods (in red) that are the only species possessing columnar limbs. The sauropod sampling made in our study also reflects partially the subgroup diversity highlighted by Carrano (2005), i.e. with non-neosauropods, diplodocoids, non-titanosaur macronarians and titanosaurs, showing skeletal specialisations that are thought to reflect functional and ecological

diversity (Carrano 2005, Vidal et al. 2020). We however acknowledge that non-titanosaur macronarians are only represented by brachiosaurid taxa in our study and that titanosaurs are only represented by three species that are probably not representative of the group, but provide a glimpse of the morphological extent found in this clade (see result and discussion). Contrastingly to in Lefebvre et al. (2022), our diplodocoid sampling does not include any rebbachisaurid, since their astragalar material is, to our knowledge, very poorly known. On another note, *Tazoudasaurus* can be distinguished from other sampled sauropods as being the only species not belonging to eusauropods (Allain & Aquesbi 2008; see discussion).

Following Lefebvre et al. (2022), the phylogenetic relationships of the sampled species were represented based on an informal consensus built with phylogenies from Peyre de Fabrègues & Allain (2020, Figure S2) and Holwerda & Pol (2018). Additional phylogenetic positions of *Amargatitanis*, *Bonatitan*, *Elaltitan*, *Lapparentosaurus*, *Tangvayosaurus* and *Vouivria* were informally added following Gallina et al. (2022), Salgado et al. (2015), Mannion & Otero (2012), Pol et al. (2011), Royo-Torres et al. (2021) and Mannion et al. (2017), respectively. Following Lefebvre et al. (2022), specimens attributed to "*Barosaurus africanus*" (whose taxonomic attribution remain dubious, see Remes 2009) are placed at the base of a polytomy of the node [Neosauropoda+*Turiasaurus*] in the phylomorphospace analysis. Similarly, a non-sauropodan sauropdomorph astragalus from Los Colorados formation was tentatively attributed to *Riojasaurus* for the purpose of the phylomorphospace analysis (see results) but do not constitute a formal taxonomic attribution.

Landmark acquisition

The shape information of sampled astragali was comprehensively captured using standard 3DGM procedures. A set of five anatomical landmarks and associated semilandmarks of curves was first defined (Table S2) and digitized for each 3D model using IDAV Landmark software (Wiley et al. 2005). A repeatability procedure was conducted on anatomical landmarks by digitizing 10 times

three closely related specimens (belonging to *Dicraeosaurus*). A generalized procrustes analysis (GPA; see Gower 1975, Rohlf & Slice 1990; see also geometric morphometrics section), followed by a principal component analysis (PCA; see geometric morphometrics section) permitted to verify (Fig. S1) that the intra-individual variability (measurement error) was lower than inter-individual variability (morphological variation). Curve semilandmarks were resampled and evenly spaced using the function from Botton-Divet et al. (2016) and reprojected to the closest point of the 3D model using the 'closemeshKD' function of the package Morpho version 2.11 (Schlager 2017) in R version 4.3.1 (R Core Team 2023). Surface semilandmarks were warped on all 3D models thanks to a template corresponding to the model of *Tazoudasaurus*. Concretely, surface semilandmarks were manually placed on the template in IDAV Landmark software, and were then warped on each 3D model using the 'PlacePatch' function of the package Morpho. A sliding procedure was performed on the sliding semilandmarks of curves and surfaces following the protocol of Gunz et al. (2005, see also Gunz & Mitteroecker 2013), minimizing the bending energy of a thin-plate spline, first between each specimen and the template ('relaxLM' function in Morpho; iterated five times), then between the result for each specimen and the consensus of the dataset ('slider3d' function in Morpho; iterated five times).

Geometric morphometrics

The slid landmarks' configurations were superimposed thanks to a GPA, removing original position, orientation and scaling information of models, using the 'gpagen' function of the geomorph R package version 4.0.5 (Baken et al. 2021). A PCA was then performed on this highly multivariate dataset, maximizing explained variation within a reduced set of uncorrelated axes, the principal components (PC), constituting a shape space. After removal of titanosaurs (because of their extremal position in the preliminary morphospace, their late stratigraphic occurrence and their probable insufficient representativeness of the clade; see results and discussion), phylogenetic relationships of specimens were projected for visual analysis on this shape space, resulting in a

phylomorphospace. Both PCA and phylomorphospace procedures were performed using the 'gm.prcomp' function of the package geomorph. A thin-plates splines analysis (see Mitteroecker & Gunz 2009) was conducted on the first three PCs, allowing the quantified visualisation and comparison of shape changes occurring along each axis. To do so, positive and negative extreme conformations of analysed PCs were mapped on the meanshape conformation. First, a 3D model of the meanshape was obtained by mapping its landmark conformation on a specimen from the dataset. We chose here the *Tazoudasaurus* model, following criteria of Lefebvre et al. (2022) (i.e. quality of preservation, minimal number of features that are too specific and could produce visual artefacts). Still, the specimen showed a few specific structures (*e.g.* presence of a foramen) that might have led to visual artefacts obscuring biological interpretations. Therefore, we prevented any potential artefact by beforehand applying laplacian smoothings to the 3D model (globally and on the mentioned area with the foramen) using Meshlab. Each extremal landmark conformation mapped on the meanshape resulted in a corresponding 3D model that was exported using the 'vcgPlywrite' function of the Rvcg R package (Schlager 2017). The resulting extreme conformations of PCs mapped on 3D models were then compared by superimposition in Meshlab. Orientation was standardized according to the meanshape model, which was positioned so that its lateral articulation faces the lateral side, and that the articular surface of the astragalar ascending process appears upwards and horizontal (i.e. the ascending process faces the proximal side). 3D visualisations were illustrated in the following figures in orthographic view. Complementarily, a Neighbour-Joining (NJ; Saitou & Nei 1987) was computed on the euclidean distance matrix computed using the first PCs axes representing the first 90% of the total variation, in order to provide a global overview of specimen clustering relatively to their global similarity.

Allometry

We aimed to explore the relationship between size and shape variation, or allometry (see Klingenberg 2016). As it is thought that the columnar limb architecture has a substantial impact in

weight-bearing efficiency, Lefebvre et al. (2022) tested the hypothesis that size acted differently on shape variation between columnar sauropods and non-columnar sauropodomorphs, with results suggesting that allometric patterns seen in the tibia and fibula (bones directly connecting the astragalus) were indeed different between these two functional groups.

We thus performed a Procrustes ANOVA (see Goodall 1991, Adams & Otarola-Castillo 2013) testing if two factors, size (through the logarithm of specimens' centroid size) and group (*i.e.* limb architecture category: columnar or not), are significantly correlated to shape variation. Such design also allows testing for the significance of an interaction between those two factors. A significant size/group interaction with shape would signify that the allometric trajectories of columnar and non-columnar taxa do not share a common slope, *i.e.* that their allometric patterns differ. A non-significant result would fail to reject – and therefore suggest – homogeneity of slope between the two groups (Lefebvre et al. 2022). If so, an additionnal permutation test stressing difference in trajectory intercepts is subsequently performed, using the function of Piras et al. (2011). This test aims to detect distinct trajectories sharing a common allometric slope coefficient (see procedure in Esquerré et al. 2017). Intercept test is performed at the smallest value of centroid size in our sample rather than at the origin, as we do not have neonates in our sample (following Ferreira-Cardoso et al. 2020). Procrustes ANOVA was performed using the 'procD.lm' function from the package geomorph. Both Procrustes ANOVA and intercept test were run with 10,000 iterations. Allometric variation common to both groups was visualised by performing a TPS analysis on a pooled multivariate regression of shape variables on size, corrected for group means (representing the Common Allometric Component [CAC], Mitteroecker et al. 2004; see also Klingenberg 2016). This step was conducted using 'CAC' and 'restoreShapes' functions of the Morpho package.

Evolutionary rates and stratigraphic uncertainty

As with the morphology of other limb bones (Lefebvre et al. 2022), astragalar shape is expected to be strongly associated with sauropodomorph evolutionary history, considering how the acquisition

of columnar architecture is thought to have had a strong impact on the evolution and diversification of sauropods (see e.g. Wilson & Sereno 1998). We thus estimated the evolutionary rates of astragalar shape variation across sauropodomorph phylogeny by performing a phylogenetic ridge regression. This phylogenetic comparative method computes a rate for each branch, without relying on an a priori model of evolution, and was explicitly thought to be applied in studies with fossil taxa (Castiglione et al. 2018). With such estimates, we aimed to test the occurrence of significant changes in evolutionary rates across sauropodomorph phylogeny.

For this analysis, specimens from the phylomorphospace analysis were used, but those with unclear and/or possibly dubious taxonomic attribution ("*Barosaurus africanus*", indeterminate astragalus from Los Colorados and some specimens with dubious position in NJ analyses, see results) were pruned. We adopted here a conservative approach minimizing the risk to mix signal from different taxa. Next, specimens from the same genus were averaged to represent a single terminal node in the tree. We gathered updated stratigraphic intervals of occurrence for each represented species, relying on recent literature (Allain & Aquesbi 2008, Remes, 2009, Tschopp et al.2015b, Mannion et al. 2017, Royo-Torres et al. 2017, Pol et al. 2021, Gallina et al. 2022, Langer et al. 2022, Otero & Peyre de Fabrègues, 2022; see SD1), to time-calibrate our phylogenetic tree. However, such intervals mostly represent a temporal uncertainty (sauropodomorph taxa being known often from a single locality) rather than a delimitation of species' period of existence. To assess sensitivity to stratigraphic uncertainty, we then used the 'timePaleoPhy' function, from the R package paleotree (Bapst 2012), setting date treatment as 'MinMax'. By this way, we generated 1000 trees whose terminal branch lengths were randomly drawn from a uniform distribution bounded by minimal and maximal ages for each species. Internal nodes' minimal ages were constrained to not be younger than the youngest possible occurrence boundary of the oldest known representative of the given clade. This procedure was applied, taking most recent literature into account, for nodes representing: Saurischia and Sauropodomorpha (cf. Langer et al. 2018), Sauropoda (cf. Viglietti et al. 2018), Neosauropoda (cf. Dai et al. 2022, Bajpai et al. 2023), Diplodocoidea and

Dicraeosauridae (cf. Bajpai et al. 2023), and Macronaria (cf. Dai et al. 2022). The node including all eusauropods in our study (*i.e.*, *Lapparentosaurus* and *Turiasaurus* + neosauropods, see Figure 1) was not constrained, as it does not represent the clade including all known eusauropods. Indeed, *Lapparentosaurus* is currently identified as a non-neosauropod eusauropod, but its precise position remains labile (see *e.g.* Läng & Mahammed 2010, Pol et al. 2011, Mannion et al. 2013, 2019, Royo-Torres et al. 2017, 2021). Although a recent study (Pol et al. 2020) confidently gave to some early patagonian eusauropods (*Bagualia, Patagosaurus* and *Volkheimeria*) a Toarcian age, recent phylogenies (*e.g.* Mannion et al. 2019, Royo-Torres et al. 2021) find *Lapparentosaurus* as closely related to younger taxa, such as *Jobaria*, hence more closely related to turiasaurs and neosauropods than to eusauropods deriving earlier (e.g. *Bagualia, Patagosaurus* and *Volkheimeria*). Other nodes were not constrained as our analysis sampled their oldest known representative. Branch lengths were estimated by minimal branch length ('mbl'; Bapst, 2012) method, setting a minimal value of 1Ma to them. To assess sensitivity to this *ad hoc* decision, we also ran our analyses setting minimal length at 0.1, 0.5, 2 and 3 My, generating for each case 200 random trees. For illustrative purposes, we also generated two calibrated trees with fixed branch lengths according to first (FAD) and last (LAD) possible occurrence dates for each species, respectively, using a minimal branch length of 1My.

Phylogenetic ridge regression was performed using 'RRphylo' function from the RRphylo R package (Castiglione et al. 2018). Significance of shifts in rates of evolution were assessed relying on the 'search.shift' function from the same package, under the 'clade' condition, which compares the mean rate of a clade to the mean rate of the rest of the tree. The function considered clades that included two to half of the species represented in the tree. Those two functions were applied to every generated tree in this study to assess sensitivity of results to each randomized parameter. We compiled the number of times the 'seach.shift' function detected a node showing a shift towards significantly higher ($p>0.975$) or lower ($p>0.025$) rates.

Results

Analysis 1 (all specimens included)

Specimens' distribution across the NJ tree discriminates all non-sauropod taxa, clustering on the right extremity, from neosauropod taxa, on the left one, and non-neosauropod sauropods plotting in between (Fig. 2A). Titanosaurs (*Tangvayosaurus*, *Bonatitan* and *Elaltitan*; subgroup 4 in Fig. 1) departs separately from other taxa along a particularly long terminal branch, suggesting unique morphologies in those sampled species. Besides those three taxa, a trend discriminating brachiosaurids (*Giraffatitan, Vouivria*; subgroup 3 in Fig. 1) and diplodocoids (*Amargatitanis, Apatosaurus, Dicraeosaurus*, *Diplodocus*; subgroup 5 in Fig. 1) is discernible, although one specimen of *Giraffatitan* (MB.R 2559) and one of *Dicraeosaurus* (MB.R 2557) mismatch in the other cluster. All specimens previously attributed to "*Barosaurus africanus*" appear as plotting in the diplodocoid cluster. The indeterminate non-sauropod sauropodomorph from Los Colorados Formation appears to be more closely similar to the specimen attributed to *Riojasaurus* than to *Lessemsaurus* or *Coloradisaurus*. We hence attribute this specimen as possibly belonging to the genus *Riojasaurus* for the next phylomorphospace analysis (but this does not constitute a formal taxonomic attribution).

Analysis of the first three PCs and associated shape deformation are dominated by the particular morphologies of the three titanosaurs taxa (Fig. 2B, see description in SD2 part a), which suggest the existence of a high, yet undersampled, morphological variability among this major morphofunctional group (see Carrano 2005). As our study focused on the impact of the acquisition of columnarity on astragalar shape, and associated first steps of morphological diversification within sauropods, we therefore chose to exclude those specimens from next analyses.

Analysis 2 (titanosaurs removed)

Specimens distribution in the NJ tree is roughly similar when removing titanosaur taxa from the analysis, with a marked discrimination between non-sauropod and sauropod taxa (Fig. 3). *Turiasaurus* plots more closely to *Vouivria* and other brachiosaurids than in the previous tree (Fig. 2A). Among neosauropods, the distinction between brachiosaurids and diplodocoids is also discernible, with the same mismatch of MB.R 2557 and 2559, again questioning the validity of their taxonomic attribution.

The first three PCs of the phylomorphospace represent 65.26% of the total variation (Fig. 4). The first PC axis contributes to 45.03% of it, and discriminates columnar sauropods (and more particularly, eusauropods) from the positive extremity to around the origin, from non-columnar sauropodomorphs and *Herrerasaurus*, on the negative side (Fig. 4A). Congruently with the NJ analysis (Fig. 3), *Tazoudasaurus*, sister-taxon of all other sauropods (subgroup 1 in Fig. 1), and the only non-eusauropod sauropod in our analysis, plots more closely to non-sauropodan sauropodomorphs than to neosauropods. Within the sauropod cluster (Fig. 4A), diplodocoids and "*Barosaurus africanus"* specimens tend to plot on the most positive side of the axis and to split apart from brachiosaurids and non-neosauropod eusauropods (*Lapparentosaurus*, *Turiasaurus*; subgroup 2 in Fig. 1), excepting the two dubious specimens highlighted in the NJ analysis (Fig. 3).

TPS analysis (Fig. 4B)*:*

General outline: The shape at the negative extremity has a subrectangular general outline in proximal view, with a main body slightly larger medially than laterally. In this same view, its anterior border shows a marked concavity, and its posterior border a marked convexity. The medial border is well-developed and gently concave in this same view and the lateral border is rather poorly developed. The main body of the negative shape is rather homogeneously thick along the mediolateral axis in posterior view, with a subhorizontal distal outline.

Relatively to the negative extremity, the shape at the positive extremity is considerably more robust and has a subtriangular general outline in proximal view, with a main body considerably more

developed laterally than medially. In this same view, the convex anterior border joins the posterior one to form a medial apex, hence with no clearly distinguishable medial border. The lateral border is, in proximal view, considerably developed. The shape of the positive extremity is wedge-shaped *sensu* Wilson & Sereno (1998) in posterior view (*i.e.* with a main body decreasing in thickness from lateral to medial direction), with a strongly bevelled outline.

Distal surface: The distal surface, delimited by the median ridge, has a saddle-shaped outline in the negative shape, *i.e.* centrally concave and convex at extremities along the mediolateral axis, while it is generally convex in the positive shape, but with a central concavity disturbing the outline regularity. The distal articular surface (distal roller *sensu* Bonnan 2005) is subdistally oriented in the negative shape, while it is anterodistally oriented in the positive shape. This variation in orientation is particularly visible in medial and in anterior views, where only the distal surface is visible in the positive shape (but see discussion part 1.1).

Lateral surface: The lateral articular surface is, in the negative shape, oriented laterally so that it is not visible in posterior view. In lateral view, the lateral articular surface is almost flat and its rather complex outline appears trilobate: proximally, the outline (of the ascending process) is flat but slightly inclined toward the anterior direction. Next (anteroproximally), a small concavity occurs and is followed by a large convexity corresponding to the border of the rounded distal surface. Distally, it is followed by a small concavity, followed by a small convexity. A last and marked posterior concavity delimits the lateral border linking the main body with the ascending process.

Relatively to the negative extremity, the lateral articular surface is in the positive shape more posterolaterally oriented and partly visible in posterior view. In lateral view, it is much more developed and markedly concave. Its outline is subsquared, and marked by a low distal bulge particularly swollen laterally.

Proximolateral surface (Ascending process and posterior fossa(e)): The ascending process of the negative shape is slightly more bevelled in lateral view than the one of the positive shape. In the negative shape, and similarly to proportions of the main body, the ascending process is

proportionally more developed along the mediolateral axis, while it is rather poorly developed along the anteroposterior axis. In proximal view, the posterior crest of the ascending process is almost orthogonal, *i.e.* rather horizontal laterally and vertical in its medial part connecting with the main body. Anteriorly, the ascending process is separated from the distal articular surface by a slightly concave triangular area. The posterior border of the ascending process is marked by a large fossa, delimited medially from the rest of the main body by a low ridge (*i.e.* the medial part of the posterior crest), and laterally from the lateral articular surface by a sharp ridge. In the positive shape, and similarly to proportions of the main body, the ascending process is proportionally less developed along the mediolateral axis, and is more extensively developed along the anteroposterior axis. In proximal view, the posterior crest of the ascending process is sigmoidal, with its lateral part being convex posteriorly and its medial part, joining the main body, being concave. Anteriorly, the ascending process directly contacts the distal articular surface. The fossa posterior to the ascending process is split in two subfossae by a crest extending to the posterior side of the median ridge. The junction between this crest and the posterior border of the median ridge is marked by a bulge. The medial subfossa is smaller but deeper, and its elliptic outline is sharply delimited. The lateral subfossa is larger and shallower hourglass-shaped, and with more subtly delimited medial and lateral margins.

Proximomedial articular surface: In the negative shape, the medial part of the main body, contacting the medial part of the tibial distal end, is elongated mediolaterally. Its proximal surface is concave, while its medial border (*i.e.*, the medial part of the median ridge) is thick proximodistally. The posteromedial part is also very developed and tends to project proximally. In the positive shape, the medial part of the main body is strongly reduced antero- and posteromedially. Its proximal surface is flatter (although inclined as described before), and the medial border is thin proximodistally.

The second PC axis contributes to 12.1% of the total variation (Fig. 4A) with no clear clustering pattern. *Panphagia* plots alone at the negative extremity, while non-sauropodan sauropodiforms (*Mussaurus* and *Lessemsaurus*) plot at the positive one. In between, other taxa are spread around the origin, but brachiosaurids plot only in negative coordinates (excepting the dubiously attributed specimen). Morphological variation along this axis (Fig. 4C) are described in SD2 part b.

The third PC axis contributes to 8.13% of the total variation (Fig. 4A). Almost all brachiosaurids specimens, the non-neosauropods sauropods and *Mussaurus* plot on negative coordinates, *Vouivria* and *Turiasaurus* occupying the negative extremity. *Herrerasaurus* plots alone on the positive extremity. The remaining taxa spread around the origin, albeit the majority of the specimens are found in positive coordinates.

TPS analysis (Fig. 4D)*:*

General outline: The shape at the negative extremity is mediolaterally elongated. It has a particular outline in proximal view, with a noticeably extensive anteromedial apex, a straight anterior border, and a posterior one marked by a pronounced convexity (*i.e.* corresponding to the bulge marking the intersection between the crest of the posterior fossa and the median ridge). In anterior and posterior views, the distal outline is not bevelled, but could be interpreted as such if slightly rotated anteriorwards (see discussion part 1.1). Relatively to the negative one, shape at the positive extremity is more robust and is subrectangular in proximal view. Medially, the border is only gently convex with antero- and posteromedial parts being almost equally developed. The anterior border is slightly concave, whereas the posterior one is gently convex. The main body of the positive shape is rather homogeneously thick along the mediolateral axis while being slightly bevelled in posterior view.

Distal surface: The distal surface is in the negative shape slightly convex with a small medial concavity disturbing the outline regularity, whereas it is saddle-shaped in the positive shape. The

distal articular surface is slightly more anterodistally inclined in the negative shape than in the positive one.

Lateral surface: In the negative shape, the lateral articular surface is concave and elongated anteroproximally to posterodistally. Its outline is elliptical and is marked by a rather high bulge. In the positive shape, the lateral articular surface is oriented more proximolaterally, being partly visible in proximal view. It is also partly visible in posterior view. Its outline is almost pentagonal and constituted of subtle concavities and convexities in lateral view. The outline is concave and is slightly marked by a blunt ridge swollen laterodistally.

Proximolateral surface (Ascending process and posterior fossa(e)): In the negative shape, the ascending process is well-developed anteroposteriorly on the lateral part of the astragalus. It is also noticeably developed laterally, the outline of the lateral border being concave in proximal view. Its proximal surface is rather horizontal, the posterior crest being directed posteriorly. In proximal view, the posterior crest is sigmoidal, with its lateral part being convex posteriorly and its medial part, joining the main body, being concave. Anteriorly, the ascending process directly contacts the distal articular surface. The fossa posterior to the ascending process is split in two subfossae by a crest extending to the posterior side of the median ridge. The junction between this crest and the median ridge is marked by a prominent bulge. The medial subfossa is very small and concave with a well-delimited elliptic outline. The lateral subfossa is very large and concave, and is hourglass-shaped, although its four margins are subequal in size (the proximal and distal ones being slightly longer than the medial and lateral ones). The medial and lateral margins are rather sharply delimited. In the positive shape, the ascending process is slightly narrower mediolaterally in proximal view, and is slightly less developed anteroposteriorly. Its proximal surface is more steeply oriented, its posterior crest being directed posteroproximally. In proximal view, the posterior crest is slightly varying mediolaterally, being rather convex laterally and concave medially. In posterior view its outline is abruptly decreasing in height in the medial direction. Anteriorly, the ascending process is separated from the distal articular surface by a slightly concave triangular area. The

posterior border of the ascending process is marked by a deeply concave and large fossa, delimited medially from the rest of the main body by a low ridge (*i.e.* the medial part of the posterior crest), and laterally from the lateral articular surface by a sharp ridge.

Proximomedial articular surface: In the negative shape, the medial part of the main body is elongated mediolaterally, but reduced posteromedially. Its proximal surface is angled, being inclined in its anterior part and horizontal in its posterior part. The medial border is thin proximodistally. In the positive shape, the medial part of the main body is rather reduced medially, but not decreasing posteromedially. Its proximal surface is concave, with a noticeably steeper transition with the proximal surface of the ascending process. The medial border is particularly thick proximodistally.

Analysis of Allometry

Relying on Procrustes ANOVA results (Table S3), we found a significant effect ($p < 0.05$) of both size and columnarity on astragalar shape. R^2 values changed from a 10% delta, depending on which factor is incorporated first in the model. Z scores did not change much for columnarity whether incorporated first or second in the model (~3.7 in both cases), while Z scores decreased for size when it was incorporated second in the model, although remaining high (from 3.2 to 2.2). The interaction of the two factors did not have a significant effect ($p = 0.13$) on shape, therefore failing to reject the hypothesis that columnar and non-columnar specimens share a common allometric pattern. The subsequent intercept permutation test did not yield significant results ($p = 0.12$), therefore failing to detect two distinct parallel trajectories.

Based on those results, we computed the common allometric component to both columnar and non-columnar taxa (Fig. 5A). When size increases (Fig. 5B), the main body is proportionally more elongated, while being less developed anteroposteriorly and thinner proximodistally, the distal surface being flatter in its anterior part. The lateral articular surface is proportionally smaller, especially proximodistally, while being slightly more sharply outlined. The ascending process is

more elongated and less developed anteroposteriorly while remaining high. The lateral area of the posterior fossa is more extended mediolaterally, while the medial part is smaller and shifts anteromedially. The bulge of the posterior margin of the median ridge is more developed and shifts more medially. The proximal surface of the medial part of the main body is slightly more concave, while the medial extremity becomes considerably thinner.

Analysis 3 (titanosaurs and dubiously attributed specimens removed)

Posteriorly to the previous analysis, we pruned specimens whose taxonomic attribution was indeterminate and/or doubtful regarding our results (see notably fig. 2B and 3) and averaged specimens belonging to the same genus (see Material and Methods).

Phylogenetic ridge regression: No obvious pattern of rate variation emerges from results obtained for FAD (oldest possible stratigraphic occurrence arbitrarily chosen) and LAD (youngest one) topologies (Fig. 6A). Comparatively, evolutionary rates computed for terminal taxa seemed visually higher than those of internal nodes when the regression was run with the LAD topology, although some rates for internal nodes (*e.g.* node 24 corresponding to Sauropodiformes) were relatively higher with the FAD one. Absolute evolutionary rates were lower with LAD topology, comparatively to rate obtained with FAD one (Fig. 6B). The distribution of rates is indeed differently structured between the two runs: while half of the nodes have had an estimated rate above the median with the FAD topology, only a quarter of them were superior to this threshold with the LAD one, with some strong disparities like for nodes 23 to 25. Conversely, terminal taxa tended to have higher rates under the run with the LAD topology. A strong discrimination is indeed visible in this case, with 6 out of 8 values above the upper quartile being rates of terminal taxa, and 7 out of 8 values under the lower quartile being rates of internal nodes.

No significant shift was found whether the FAD or LAD topology was used, when no randomization procedure was conducted accounting for stratigraphic uncertainty (Table 1).

Sensitivity to stratigraphic uncertainty: When conducting the randomization procedure, we found significant shifts at the nodes 27, 28, 29, and 31 in 51.4%, 47.5%, 19.2%, and 4.9% of iterations, respectively (Table 1). The majority of those results indicated a significant shift to lower evolutionary rates, whereas a tiny proportion of shifts to higher rates was found for nodes 29 and 31.

Sensitivity to branch length reconstruction: We found, when varying the "mbl" parameter, significant occurrences of shift in evolutionary rates for the same nodes 27, 28, 29 and 31 (Table 2). When increasing the "mbl" value, we tended to find a considerably higher proportion of significant shifts to lower rates. For example, a 35.5% proportion was found for the node 27 when mbl was set to 0.1Ma, to up to 93.5% for this same node when mbl was set to 2Ma. A tiny proportion (<5%) of shifts to higher rates were found for nodes 29 and 31 for small mbl values, which tended to decrease to 0% at higher mbl values. Over the 200 iterations for a given mbl value, variability in evolutionary rates' estimation was large at small mbl values, with an average 78.28% coefficient of variation when mbl was set to 0.1Ma, and tended to decrease with higher mbl values, with an average 22.31% at a 3Ma mbl value (Table 3). Maximal variability for a node also tended to decrease from 244.35% with 0.1Ma value to 54.18% with 3Ma value, while minimal variability tended to remain stable (around 3.5-5.5%).

Discussion

Part 1: How distinguishable are columnar sauropods?

1.1 Distinctions between eusauropods and non-sauropodan sauropodomorphs

Similarly to in limb long bones (Lefebvre et al. 2022), our results show that the shape of the astragalus in columnar sauropods is significantly different from that in other non-columnar taxa (Table S3). More precisely, we highlighted here a major trend of morphological variation (fig. 4A,

565 B) distinguishing eusauropods (Morphotype C.1 and C.2 in Fig. 7, corresponding to all sampled
566 sauropods excepting *Tazoudasaurus*) from non-sauropodan sauropodomorphs (Morphotype A in
567 Fig. 7) with the following features:
568 - *General proportions* (feature 1 in Fig. 7 and Appendix S1A): eusauropod astragalus differs
569 drastically from other sauropodomorphs by being relatively mediolaterally short and pronouncedly
570 asymmetric, the lateral half being considerably more developed anteroposteriorly than the medial
571 one (1:c in Fig. 7). This corresponds to the “wedge-shaped” condition described in Wilson &
572 Sereno (1998). Contrastingly, the astragalus in non-sauropodan sauropodomorphs is relatively
573 rectangular, elongated mediolaterally (1:a in Fig. 7).
574 - *Shape of the distal surface* (feature 2 in Fig. 7 and Appendix S1A): In eusauropods the distal
575 articular surface is generally smoothly convex, giving a rather regular articular surface (2:c in Fig.
576 7), often named “distal roller” (Bonnan 2005). This condition differs from non-sauropod
577 sauropodomorphs, whose distal surface appears anteriorly saddle-shaped, that is, centrally concave
578 and convex in its medial and lateral extremities (2:a in Fig. 7). Both morphotypes appear to have a
579 convex posterior part for the distal surface.
580 - *Orientation of the distal surface* (feature 3 in Fig. 7 and Appendix S1A): The distal surface is
581 quantitatively distinguishable in eusauropods as having in average a more anterodistal orientation
582 (3:c in Fig. 7) than in non-sauropodan sauropodomorphs, whose surface appear more vertically-
583 oriented (3:a in Fig. 7). In practice, however, the orientation of the distal roller in an anatomically
584 relevant position may be hard to assess from an isolated astragalus. Anatomically, the position of
585 the astragalus at rest obviously depends of its relative position to the distal ends of the hindlimb
586 zeugopod. This is partly linked to the inclination of the ascending process, which is assumed to be
587 almost horizontal in the literature (see *e.g.* Wilson & Sereno 1998, Bonnan 2005). However, such
588 feature may vary across eusauropod species, consistently with variability of the corresponding
589 articular surface on the distal end of the tibia (see *e.g.* Janensch 1961, Lefebvre et al. 2022) that
590 suggests that the articular surface of the ascending process is rarely horizontal in an anatomically

relevant position. Additionally, the contacting areas of astragalus with the tibia (ascending process, medial half of the main body) may vary in their proportional contribution of their anterior and proximal faces in such a way that is hard to assess without physically connecting the astragalus to the tibia (see *e.g. Vulcanodon* in Cooper 1984, but see also Wilson & Sereno 1998; *Camarasaurus* in Wilson & Sereno 1998, *Erketu* in Ksepka & Norell 2006). Finally, the perceived degree of inclination can be accentuated or diminished by how the observer sets its orientation, such as in our study, where extremal shape variations of the three described axes were by necessity standardized together relatively to the meanshape, thereby impacting two-dimensional illustrations (Fig 4). Such bias is prevented when examining specimens under the 3DGM framework, or may be minimized qualitatively by direct observations of real specimens, but will inevitably affect (two-dimensional) reference illustrations published in the literature (see *e.g.* variation in orientation nomenclature in Cooper 1984 and its discussion by Wilson & Sereno 1998; in Wilson & Sereno 1998 and its discussion by Bonnan 2005; see also nomenclatures in Allain & Aquesbi 2008; Mannion et al. 2013, 2019, Tschopp & Mateus, 2017, Royo-Torres et al. 2021). This reflects the difficulty to adopt a stable standardisation when examining biological objects showing strong variations of relative orientation such as with the sauropodomorph astragalus.

- *Presence/absence of the anterolateral triangular area as a reliable proxy associated with distal roller orientation* (feature 4 in Fig. 7 and Appendix S1A): Our analysis highlighted that eusauropods were distinguishable by lacking a triangular anterolateral area (4:c in Fig. 7) found in non-sauropodan sauropodomorphs that appears to bear a concavity (4:a in Fig. 7) bordered by an inferior and a superior ridge in best preserved specimens (*e.g. Coloradisaurus* [Apaldetti et al. 2013]; *Riojasaurus* [see specimen illustrated by Novas 1989, fig.4.5]; *Plateosaurus* [see specimen illustrated by von Huene 1926 table V-8b]). The absence of this area is a synonym of direct connection between the distal roller and the proximal side of the ascending process, which necessarily implies a steeper angle between these two articular surfaces. Therefore, assessing the

presence/absence of this intermediary area in sauropodomorphs can act as a less sensitive but more objective proxy reflecting variation of the distal roller relatively to the tibia (see also section 1.3).

- *Lateral articular surface* (feature 5 in Fig. 7 and Appendix S1A): The lateral surface outline is much simpler in eusauropods, being subsquared to subpentagonal (5:b in Fig. 7). This contrasts with the “trilobate” condition found in non-sauropodan sauropdomorphs (5:a in Fig. 7), whose concavities reflect the presence, anteriorly, of the anterolateral triangular surface (see above), and distally, of depressions and projections interlocking with the calcaneum (see Novas 1989, fig 4.8 and 4.11). This latter area is replaced in eusauropods by a swelling of the distal border, which may be related to the proportional reduction/disparition/non-ossification/fusion of an isolated calcaneum, depending on cases and interpretations (Bonnan 2000, see also part 4.3).

Additionally, the lateral surface of eusauropods is distinguished by being markedly concave, and its outline is well-defined by a ridge. Finally, the orientation of the lateral articular surface appear to vary, but is probably reflecting a trend within sauropods (see section 2.1)

- *Ascending process* (feature 6 in Fig. 7 and Appendix S1A): In eusauropods, it is slightly less bevelled and more developed anteroposteriorly than mediolaterally (6:b in Fig. 7), proportionally following the same trends as the general proportions of the main body. This condition contrasts with the more bevelled and more mediolaterally developed ascending process seen in non-sauropodan sauropodomorphs (6:a in Fig. 7). However, as stated above for the distal roller, such variation of orientation can be sensitive to angle of observation, and also substantially variates within-groups. This questions the reliability of the popular phylogenetic character, proposed by Wilson & Sereno (1998), coding for the posterior extension of the ascending process relatively to the posterior border of the astragalus (see section 1.3 for further details). Although being relevant and particularly perceptible *e.g.* in the *Camarasaurus* specimen illustrated by Wilson & Sereno (1998), or in our analysis with *e.g. Turiasaurus*, the signal is more equivocal when considering diplodocid taxa, or when anatomical orientation of the specimen is unclear.

- *Crest dividing the posterior fossa in two subfossae* (feature 7 in Fig. 7 and Appendix S1A): As recovered in numerous phylogenetic studies (*e.g.* Wilson & Sereno 1998, see also sections 1.3 and 2.2), all eusauropods have a posterior fossa partitioned in two subunits by a crest (7:b in Fig. 7) extending anteroposteriorly and posteriorly reaching the median ridge on a point marked by a developed bulge. This crest is absent in non-sauropodan sauropodomorphs (7:a in Fig. 7)

- *Medial half development* (feature 8 in Fig. 7 and Appendix S1A): Eusauropods depart from the condition seen in non-sauropodan sauropodomorphs by having a reduced medial part of the main body. It usually consists in a triangular medial apex (8:b in Fig. 7), whose development may vary, while non-sauropodan sauropodomorphs have a squared medial half, with strongly developed antero- and posteromedial corners (8:a in Fig. 7). Distally, this variation is associated, in eusauropods, with a strong decrease in proximodistal thickness of the main body, particularly noticeable in medial view, which contribute to the distinctive “wedge-shaped” condition. Proximally, the surface articulating with the tibia appears flatter in eusauropods, despite some within-group variation.

1.2 Condition in Tazoudasaurus *and relevance for the evolution of the sauropod bauplan*

Tazoudasaurus (Morphotype B in Fig. 7) is the oldest sauropod represented in our sampling, and is the only sauropod not belonging to eusauropods. While clearly having a columnar limb architecture, this taxon plots in-between eusauropods and non-sauropodan sauropodomorphs morphological clusters (Figs 3, 4A), as one may expect given its phylogenetic position.

Tazoudasaurus indeed shares with eusauropods, to some extent, a wedge-shape general morphology, notably marked by some degree of proximodistal flattening of the medial half (but to a lesser extent than seen in eusauropods; 1:b in Fig. 7), meanwhile being rather medially rectangular, mediolaterally elongated and with a concave anterior margin in proximal view, as in non-sauropodan sauropodomorphs (8:a in Fig. 7; see also Allain & Aquesbi 2008, fig. 30 C-F). The distal surface appears slightly more oriented anterodistally than in the typical condition of non-

667 sauropodan sauropodomorphs, but not to the extent of the typical condition of eusauropods (3:b in
668 Fig. 7); moreover, it is saddle-shaped (2:a) and possesses an anterolateral triangular surface (4:a;
669 see also Allain & Aquesbi 2008, fig. 30 C-D), separating the ascending process and the distal
670 articular surface, as in non-sauropodan sauropodomorphs. Laterally, the lateral articular surface
671 outline in *Tazoudasaurus* is similar to the archetypal condition seen in eusauropods, with a well-
672 marked sharp ridge delimiting a subcircular concavity (5:b in Fig. 7), and with a swollen distal part.
673 This articular surface is, however, laterally oriented. The ascending process is rather not bevelled,
674 and is more developed anteroposteriorly than laterally (6:b in Fig. 7; see also Allain & Aquesbi
675 2008, fig. 30 E-F). The lateral part of the ascending process is well-developed anteroposteriorly, and
676 the posterior fossa is divided into two parts by a crest (7:b in Fig. 7), whose meeting point with the
677 posterior margin is materialized by a developed bulge, as in eusauropods (see Allain & Aquesbi
678 2008, fig. 30 A-B, E-F).
679 Taken globally, *Tazoudasaurus* bears a suite of plesiomorphic and apomorphic traits, and therefore
680 appears as an intermediary morphotype (Appendix S1A). This suggests that the acquisition of
681 columnar limbs in sauropods is linked to significant changes in astragalar morphology,
682 notwithstanding that the full set of traits characterizing the majority of species in this group (*e.g.*
683 reduction of the medial half to a triangular apex) are acquired in eusauropods. This result is
684 congruent with the rather gradual pattern found for the tibia and the fibula (Lefebvre et al. 2022),
685 which corroborates the idea that the morphological evolution related to the emergence of the
686 sauropod bauplan was more stepwise in the hindlimb than in the forelimb (Lefebvre et al. 2022).
687 This differential evolutionary scenario probably reflects contrasting selective pressures between the
688 forelimb and the hindlimb, the latter being mainly dedicated to locomotion and weight-bearing in
689 every sauropodomorphs, while the former was probably subject to a wider panel of potential
690 constraints in habitual or occasional bipeds using their forelimb for other functions (*e.g.* grasping,
691 digging). Functional diversity was, on the other hand, probably strongly reduced with the

692 acquisition of columnar limbs, which implied exclusive use of the forelimbs for locomotion and
693 weight-bearing.
694
695 *1.3 Implications for coding phylogenetic characters*
696 Phylogenetic studies including sauropod and non-sauropodan sauropodomorph taxa rely on several
697 phylogenetic characters coded for the shape of the astragalus. The most commonly coded ones
698 inform about its general proportions (Feature 1 in Fig. 7), discriminating between a wedge-shape
699 and a non-wedged shape in anterior and/or proximal views. This variation is usually quantified with
700 ratios, such as between maximal (mediolateral) width and (anteroposterior) length (in e.g. D'Emic
701 2012, Mannion et al. 2013, 2019, Carballido et al. 2017, Pol et al. 2020), and/or between width and
702 (proximodistal) height (in e.g. Mannion et al. 2013, 2019, Tschopp et al. 2015, Carballido et al.
703 2017, Holwerda & Pol 2018, Pol et al. 2020), and/or between maximal medial and lateral lengths
704 (in e.g. Mannion et al. 2013, 2019). This latter distinction is similar to the characters coding in
705 proximal view for the development of the anteromedial (in e.g. Wilson & Sereno, 1998, Wilson,
706 2002, Allain & Aquesbi 2008, Whitlock 2011, Tschopp et al. 2015, Carballido et al. 2017, Holwerda
707 & Pol 2018, Pol et al. 2020) and posteromedial corners (in e.g. Upchurch 2007, Yates 2007, Pol et
708 al. 2011, 2020, Peyre de Fabrègues & Allain 2020). Reference view is not always mentioned for
709 those characters, although a wedge-shape condition can be differentially observed in both anterior
710 and proximal views. Interestingly, the condition in *Tazoudasaurus* shows that the astragalus can be
711 rectangular in one of the two views, and wedge-shaped in the other one, with a thick medial half
712 (see morphotype B in Fig. 7 ans see Allain & Aquesbi, Fig. 30). Beyond considerations regarding
713 the angle of view, the previously mentioned measurements are often not rigorously defined (i.e. no
714 specific region is mentioned, or the measure is taken at maximum). This can potentially lead to the
715 comparison of measures which clearly do not correspond to biologically homologous structures (for
716 example, the maximum anteroposterior length is often corresponding to the medial extremity of the
717 astragalus in non-sauropodan sauropodomorphs, whereas it is usually corresponding to the lateral

718 one in eusauropods). Additionally, the lack of clear definition can potentially result in redundancy
719 of phylogenetic characters. Notably, information coded for the general proportions of the astragalus
720 might also appear in characters regarding the depth of the medial end (corresponding to feature 8 in
721 Fig. 7, and to characters coded in e.g. Upchurch 2007, Yates 2007, Mannion et al. 2013, 2019, Peyre
722 de Fabrègues & Allain, 2020, Pol et al. 2020). Phylogenetic matrices often also code for the
723 development of the ascending process (Feature 6 in Fig. 7) by quantifying its length relatively to
724 either its width (in e.g. Yates 2007, Peyre de Fabrègues & Allain 2020) or to the length of the
725 astragalus (in e.g. Wilson & Sereno 1998, Wilson 2002, Yates 2007, Allain & Aquesbi 2008,
726 Whitlock 2011, Mannion et al. 2013, 2019, Tschopp et al. 2015, Carballido et al. 2017, Holwerda &
727 Pol 2018, Peyre de Fabrègues & Allain 2020, Pol et al. 2020), or by describing its shape
728 qualitatively (in e.g. Pol et al. 2011). We therefore suggest to be cautious when defining the
729 biological structure measured to capture the general proportions (Feature 1 in Fig. 7) and the
730 developments of the medial half (Feature 8) and of the ascending process (Feature 6) in the
731 astragalus of sauropodomorphs. For instance, the anteroposterior length may be taken in proximal
732 view at the level of the junction between the ascending process (and its posterior fossa) and the
733 medial half, which is easily recognizable in every sauropodomorph. Similarly, the dimensions of the
734 medial extremity against the lateral one could be compared not only in length (as in e.g. Mannion et
735 al. 2013, 2019), but also in proximodistal height to document thickness variations (the lateral
736 measure can be taken at its maximum or at the level of the posterior fossa depending on whether
737 one want to take the ascending process into account). Measures taken on physical specimens or 3D
738 models should be obviously privileged over the ones taken on 2D illustrations, because of the lack
739 of clear standardisation in orientation.
740 The presence/absence of a crest dividing the posterior fossa in two subfossae (Feature 7 in fig. 7) is
741 well-captured by existing binary characters (in e.g. Wilson & Sereno 1998, Wilson 2002, Upchurch
742 2007, Yates 2007, Allain & Aquesbi 2008, Carballido et al. 2017, Holwerda & Pol 2018, Peyre de
743 Fabrègues & Allain 2020; Pol et al. 2020). This statement is also true for the shape of the distal

surface (Feature 2 in Fig. 7), despite being more rarely used (in e.g. Allain & Aquesbi 2008, Pol et al. 2020). We therefore suggest no particular modification in coding these two features.

On another note, our analyses highlighted some variations which probably bear an interesting phylogenetic signal. The morphology of the lateral articular surface (Feature 5 in Fig. 7) is indeed coded in some matrices (in e.g. Upchurch 2007, Yates 2007, Pol et al. 2011, Peyre de Fabrègues & Allain 2020), but for a variation (presence/absence of a horizontal shelf) regrouping most sauropodomorphs together, thereby not documenting at all the strong changes observed in relation with the emergence of the sauropod bauplan. We therefore suggest the creation of a new phylogenetic character coding for the shape of the lateral articular surface, including at least two states: trilobate, flat without outlining ridge (0); subcircular to subpentagonal, concave, outlined by a ridge (1).

The orientation of the distal articular surface (Feature 3 in Fig. 7) is not documented by any phylogenetic character; such variation is mostly discussed in morphofunctional studies (e.g. Bonnan 2005). This certainly relates to the difficulty to standardize the orientation of the astragalus in sauropodomorphs, especially when the connecting tibia is missing. However, the easier observation of the presence/absence of an anterolateral triangular surface (Feature 4 in Fig. 7) appears to be a well-correlated substitute to document this variation of orientation, despite being less sensitive. This variation is indirectly partly captured by another character found in many matrices (in e.g. Wilson & Sereno 1998, Wilson 2002, Upchurch, 2007, Yates 2007, Allain & Aquesbi 2008, Pol et al. 2011, Carballido et al. 2017, Holwerda & Pol 2018, Peyre de Fabrègues & Allain 2020, Pol et al. 2020), coding for the presence of a depression (or fossa) and/or vascular foramina in this area (i.e. “at the base of the ascending process”). The definition of this character always involves foramina, although their actual presence can be unclear (see e.g. *Coloradisaurus* in Apaldetti et al. 2014). Also, while the presence of a depression/fossa is far more clearer (and, in practice, used to code the state “present” whether there are visible foramina or not), this coding strategy usually groups taxa bearing an existing, but flat, triangular area (such as *Lessemsaurus*, *Mussaurus* and *Tazoudasaurus*)

with eusauropods (in which this particular area is absent). Considering our results, we propose to replace this character (initially proposed in Wilson & Sereno 1998 [#12], coding for the presence/absence of foramina) by a new one with three states: presence of a concave anterolateral triangular area (0); presence of a flat anterolateral triangular area (1); absence of any anterolateral triangular area: the distal articular surface is directly contacting the median border, the area is therefore indistinguishably convex (2). An ordering of this character can be plausibly considered, as one may assume that the morphological transition from a concavity to an absence (here corresponding to a convexity) shall necessarily transit by an intermediary flat state.

Last, we did not comment the presence of a pyramidal process (coded in e.g. Yates 2007, Peyre de Fabrègues & Allain 2020) as it is only seen in some non-sauropod taxa (e.g. *Coloradisaurus,* see Apaldetti et al. 2014). We only note here that this development is certainly not homologous to the development of the posterior bulge seen in sauropods. The latter structure is indeed located at a recognizable triple junction between the posterior side of the median border and the delimitation of the medial half and the posterior fossa (on a rather central position), whereas the former is situated much more medially from this meeting point.

1.4 Note on the plesiomorphic sauropodomorph morphotype

Sauropodomorph astragali are traditionally thought as being more mediolaterally elongated than in early saurischians such as *Herrerasaurus* (Novas 1989). The latter, although sharing strong similarity with non-sauropodan sauropodomorphs in our study (Fig. 3), has a blocky general outline, almost squared in proximal view. Recent discoveries of early sauropodomorphs such as *Panphagia* (Martinez & Alcober 2009, see also Müller 2021, fig.4) sampled in our study, and *Saturnalia* (Langer 2003, see also Müller 2021, fig.4), show that sauropodomorphs plesiomorphically retained the general dimensions found in early saurischians. The mediolaterally elongated morphotype subsequently appears in later taxa, and was probably acquired in taxa belonging or closely related to the clade Plateosauria. Plasticity within *Plateosaurus* (see section

3.3), however, does not help to infer when this particular morphotype appeared during sauropodomorph evolution. Future studies focused on this precise episode and thus relying on a more relevant sample (*i.e.* including more Carnian taxa, with both non-plateosaurian and plateosaurian sauropodomorphs) would provide clearer conclusions.

Part 2: Beyond columnarity: what's happening within columnar sauropods?

2.1 Morphological variation of diplodocoids, brachiosaurids and other non-neosauropod taxa.

The distribution of taxa on the phylomorphospace (fig. 4A) and NJ (fig. 3) suggests that the archetypal eusauropod morphotype (C.1 in Fig. 7, see also Appendix S1B) in fact corresponds more specifically to a subgroup within neosauropods, belonging to Diplodocoidea (subgroup 5 in Fig. 1; assuming that "*Barosaurus africanus*" specimens belong to this clade, and that MB.R2559 was incorrectly attributed to *Giraffatitan*), while other taxa (brachiosaurids, represented by morphotype C.2 in Fig. 7 and subgroup 3 in Fig. 1; *Turiasaurus and Lapparentosaurus,* subgroup 2 in Fig. 1; and assuming an incorrect attribution of MB.R2557 to *Dicraeosaurus*; see also Appendix S1B) do not show such an extreme morphology, as indicated by their intermediate occupation of the morphospace. The latter cluster also appears to differ from diplodocoid morphology along minor trends of variation (fig. 4D).

More concretely, sauropods tended to show variability for the following features:

- *The medial apex* (feature I and II in Fig. 7 and Appendix S1B), whose shape is usually triangular in eusauropods, and very reduced in *Dicraeosaurus* (I:b in Fig. 7). It is, however, generally more developed in unambiguous non-diplodocoids (I:a in Fig. 7), and even particularly deflected anteromedially in brachiosaurids (II:b in Fig. 7, as in *e.g. Vouivria,* see Mannion et al. 2017, Fig. 36) with a particularly curved apical outline in proximal view. But large diplodocoids, such as *Diplodocus* (see *e.g.* another specimen in Hatcher 1901, Fig. 20) and *Apatosaurus* (see *e.g.* another specimen in Gilmore 1936, Fig. 26), can show some degree of projection of the (undeflected, II:a in

fig. 7) medial apex, suggesting that this development may be related to size (see section 3) and/or is reduced in more inclusive group(s) within Diplodocoidea.

- *The distal swelling of the lateral articular surface outline* (feature III in Fig. 7 and Appendix S1B), appearing as particularly projected laterally in diplodocoids and in "*Barosaurus africanus*" specimens (III:c), underlying a substantial part of distal end of the fibula. This condition is thought to be lost in macronarians (Mannion et al. 2019). Our analyses corroborate this loss for brachiosaurids (III:a), but it is also seen in *Lapparentosaurus*. While a non-flat swelling is noticeable in *Turiasaurus*, it is not noticeably projected laterally in this taxon (see Royo-Torres et al. 2006, fig. 1Q, S). In contrast, *Tazoudasaurus* appears to have some degree of lateral projection (III:b in Fig. 7, see also Allain & Aquesbi 2008 Fig. 30 C-D).

- *Orientation of the lateral articular surface* (feature IV in Fig. 7 and Appendix S1B), which is facing more posterolaterally in diplodocoids and in "*Barosaurus africanus*" specimens (IV:b), while it is strictly laterally oriented in other taxa (IV:a). This feature has indeed been proposed as a synapomorphy of Diplodocoidea (Whitlock 2011).

- *Division of the posterior fossa* (feature V in Fig. 7 and Appendix S1B): All sauropods bear a crest dividing the posterior fossa in two subfossae, but their finer proportions, outline and depth vary within the group. In neosauropods, brachiosaurids show a posterior fossa predominantly occupied by the lateral fossa over the medial one (V:c), whereas an opposite trend occurs in diplodocoids and "*Barosaurus africanus*" (V:b). In this latter group, the lateral fossa can be as large as the medial fossa in large specimens (*e.g. Apatosaurus*, *Diplodocus*), to reduced to a strong keel in *e.g.* smallest *Dicraeosaurus* specimens. Finer levels of variations also occur, although not reflecting a clear phylogenetic discrimination. The medial subfossa is a bit shifted centrally in brachiosaurids and small diplodocoids and "*Barosaurus africanus*" specimens. The subfossae are well-outlined in brachiosaurids and in small diplodocoid and small "*Barosaurus africanus*" specimens, contrasting with more subtle distinctions in large diplodocoids and large "*Barosaurus africanus*" specimens. The medial subfossa appears generally deeper in diplodocoids and "*Barosaurus africanus*"

specimens, while it is as deep as the lateral subfossa in brachiosaurids; this depth disparity is more marked in smaller specimens (see section 3). In non-neosauropod taxa, *Turiasaurus* and *Lapparentosaurus* have well-outlined and equally deep subfossae, with the lateral one being much larger than the medial one. Contrastingly, *Tazoudasaurus* has the reverse condition, with the medial subfossa much larger than the lateral one (V:a in Fig. 7).

- *Bulge at the intersection between the crest of the posterior fossa and the posterior margin of the astragalus* (feature VI in Fig. 7 and Appendix S1B), which is considerably more developed proximally in brachiosaurids and in *Turiasaurus* (VI:b) than in other taxa (VI:a).

2.2 Implications for coding phylogenetic characters

Several characters are used to describe the shape of the astragalus in phylogenetic studies disentangling the within-group relationships in sauropods. As in section 1.3, some linear measurements are usually taken to describe the transverse (mediolateral) development of the astragalus (as in e.g. D'Emic 2012, Mannion et al. 2013, 2019, Carballido et al. 2017, Holwerda & Pol 2018, Pol et al. 2020). However, this variation (Feature I in Fig. 7) is substantially size-related (see section 3): for example, both large diplodocoids and macronarians can have quite elongated astragali. Similarly, astragalar capping of the tibia (coded in e.g. Mannion et al. 2013, 2019) is known to be reduced in some large sauropods (see section 4.3), which is perhaps related to a developmental pattern of ossification that might be widespread among sauropods (rather than specific to any monophyletic subgroup), hence calling for cautious use as a phylogenetic character.

Some trait variation highlighted in our study are already well-coded in matrices, such as the orientation of the lateral articular surface (in e.g. Whitlock 2011; Tschopp et al. 2015, Carballido et al. 2017, Holwerda & Pol 2018, Mannion et al. 2019, Pol et al. 2020; corresponding to feature IV in Fig. 7) and the development of the lateral swelling (in e.g. Mannion et al. 2013, 2019, Tschopp et al. 2015, corresponding to feature III in Fig. 7). A binary character is often used to code a presence/absence of the posterior bulge of the median margin (in e.g. Yates 2007, D'Emic 2012,

Mannion et al. 2013, 2019, Peyre de Fabrègues & Allain 2020, Pol et al. 2020), whereas our analyses suggest that the structure is always present, but variates in the magnitude of its development (see feature VI in Fig. 7). We here suggest that this character could benefit from a subtler assessment rather than a simple presence/absence.

We also found that the deflection of the medial apex (Feature II in Fig. 7) is usually not captured by any character. Although the shape of this structure in posterior view is coded by Tschopp et al. 2015 (character #456, see the fig. 104), its level of deflection in proximal view (as in Bonnan 2000, fig. 4) is, to our knowledge, lacking in the literature. We therefore suggest to create a new binary character coding for a not deflected (0; see Bonnan 2000, fig. 4B) or anteromedially deflected (1; see Bonnan 2000, fig. 4A) medial apex. Alternatively, one could code for the shape of the anterior border of this structure in proximal view, that can be clearly oblique (as in Bonnan, 2000 fig. 4B) when there is no deflection, or straight (as in Bonnan 2000, fig. 4A) in deflected apices.

Lastly, while the presence/absence of the crest dividing the posterior fossa is often coded (see feature 7 in Fig.7 and discussion in section 1), subtler but clearly discernible variations also occur among sauropods. While the variations highlighted in our study are multiple and complex, the main changes such as the relative proportions of a subfossa compared to the other (Feature V in Fig. 7) appear as a promising character. We suggest to code this variation with a ternary ordered character with either the medial subfossa being much larger than the lateral one (0), both subfossae being subequal in size (1; the lateral subfossa can be reduced to a strong but flat keel; empirically one subfossa [often the medial one] can be slightly larger in area), or the lateral subfossa is much larger than the medial one (2). This morphocline may be combined with the binary character coding for the presence/absence of the delimitation ridge by adding a state 3 (absence of ridge delimiting the two subfossae) whose transformation from/to state 0-2 would uniformly cost one step.

2.3 Perspectives regarding titanosaurs

The inclusion of titanosaurs permitted us to show a wide occupation of the morphospace extrema, although we only used three specimens (Fig. 2, S2). With such a small sampling size, it is impossible to extract useful biological interpretations, regarding for instance the opposite trends in ascending process development and orientation between *Elaltitan* (Mannion & Otero 2012) and *Tangvayosaurus* (Allain et al. 1999), or *Bonatitan* (Salgado et al. 2015) whose morphology is difficult to interpret relatively to its particularly small size (certainly reflecting a very early ontogenetic stage). Those three specimens have so unusual morphologies that one cannot even exclude exaggeration of their morphology by insufficient completeness and/or taphonomic distortion as confidently as for other sauropodomorphs, for which intraspecific or similar interspecific material is more abundant. Aside from these examples, despite the generally poor preservation of fairly complete titanosaurs (Cashmore et al. 2020), astragalar morphological diversity appears very high within this clade, with at least three different main morphotypes recently identified (Perez-Moreno et al. 2024). All those elements call for further investigation relying on a more robust sampling, which is needed to discuss about the evolutionary modalities occurring within this clade.

Part 3: To which extent is morphological variation related to size?

3.1 Common allometric pattern

When size increases, the main morphological variation shared by the columnar and the non-columnar groups relates to the general mediolateral elongation of the astragalus. The articular surface areas tend to reduce, which may appear counter-intuitive as large terrestrial mammals (e.g. rhinoceroses) tend to show an opposite trend (Gregory 1912; Osborn 1929; Etienne et al. 2020; but see section 4.1). However, they appear to more tightly constrain the connection with the hindlimb zeugopod.

Proximally, the tibial distal end contacts medially with a more concave medial half, and its descending process is constrained by a strong development of the posterior margin. This feature reflects a convergence between the proximal development of the posteromedial corner in large non-sauropodan sauropodomorphs, such as in *Coloradisaurus* (see Apaldetti et al. 2013, fig. 14D) and *Mussaurus* (see Otero & Pol 2013, fig. 16B), and the proximal development of the bulge materializing the meeting of the crest dividing the posterior fossa with the posterior border in large sauropods, as in *Turiasaurus* (see specimen illustrated in Royo-Torres et al. 2021, Fig. 16A, D) and *Vouivria* (see Mannion et al. 2017, fig.36D). Laterally, the surface articulating with the fibula and the calcaneum (when existing) is reduced in large specimens, but with a strongly marked outline, suggesting a tighter interlocking. In both cases, more strongly marked articular surfaces again contradict the pattern seen in large terrestrial mammals (but see section 4). Finally, the proximodistal thickness is reduced in large animals, with a flatter distal roller, that is congruent with the mammalian signal.

3.2 Discordance with hindlimb zeugopod allometric pattern

Considering the direct association of the tibia and the fibula with the astragalus, it is perhaps surprising to find results supporting the assumption of an allometric relationship common to non-columnar and columnar sauropodomorphs, whereas divergent allometric patterns where highlighted previously for the hindlimb zeugopod (Lefebvre et al. 2022). However, associated shape changes in the distal end area of those two bones appear as compatible with the size-related morphological variation of the astragalus. In the tibia, non-sauropodan sauropodomorphs show a congruent mediolateral elongation (Lefebvre et al. 2022, fig.12), while sauropod decrease in robustness was mostly affecting the descending process (Lefebvre et al. 2022, fig.13). Both groups also retained a marked development of the medial side of the fibular distal end (Lefebvre et al. 2022, fig.14, 15). This perhaps suggests that the morphological signal respectively captured for the tibial and fibular distal ends is not necessarily following the same trend as the rest of the bone (respective proximal

ends and shafts). The veracity of this statement could be clarified by analysing local shape variation of a sample of hindlimb zeugopod distal ends alone to assess more precisely their covariation with the astragalus. On another note, it was suspected that tibial and fibular allometric patterns highlighted in Lefebvre et al. (2022) could have been more reflecting a trend occurring within diplodocoids because of the strong sampling imbalance for this clade, which is not the case in the present study. In that case, the contrasting results between those two investigations thus reflect more the existence of diverging allometric patterns within some sauropod subclades rather than between all sauropods and all other sauropodomorphs.

3.3 Particular within-group implications

Phylomorphospace analysis allowed to distinguish morphotypes within sauropods (see section 2.1 and morphotypes B,C.1 and C.2 in Fig. 7). However, a part of those morphological variations were also visualised with the analysis of the common allometric component, hence meaning that they are at least partly related to size (*e.g.* feature II in Fig. 7). This result was to be expected at least within neosauropods, as macronarian species (including brachiosaurids) usually reach larger maximum sizes than diplodocoid ones. Still, size-related variation goes beyond this dichotomy, since some morphological similarity is found in distantly-related and large specimens, such as *Giraffatitan*, *Apatosaurus* and *Turiasaurus*. This allometric variation may hence relate equivalently or even more on an ontogenetic level than an evolutionary one. However, such hypothesis must be nuanced, as small specimens such as *Lapparentosaurus* showed strong CAC scores, contrasting with lower scores in specimens of similar size, such as the smallest sampled *Dicraeosaurus* (fig. 5A), showing that growth alone cannot explain all the variation related to size disparity sampled here. On the other hand, static allometry is not negligible, as phenotypic plasticity during growth is particularly documented in non-sauropodan sauropodomorphs (Sander & Klein 2005, Klein & Sander 2007, Chapelle et al. 2021, Cerda et al. 2022). Contribution of ontogeny and plasticity to the common allometric component is therefore hard to assess without explicit assessment of ontogenetic stages.

It is indeed illustrated in our study by strong disparity in CAC scores observed for the four sampled *Plateosaurus*, despite a relatively homogeneous size (fig. 5A). Two morphs are indeed discernible for this species, with the neotypic specimen showing an unusually robust morph recalling the plesiomorphic condition in early sauropodomorphs (see Müller 2021), and echoing a similar signal found in the tibia and the fibula (Lefebvre et al. 2022, figs. 12&14). Our results therefore corroborate the already strong plasticity known for this genus, assuming correct taxonomic assignment of the specimens.

To summarize, our sample cannot discriminate between the three canonical levels of allometry (that is, evolutionary, ontogenetic and static, see Klingenberg 2016) but allows our study to usefully delineate a general trend common to all sauropodomorphs, which calls further investigation seeking for finer-level and more disentangled tendencies. Among others, our work clearly calls for further investigation of allometric trends within neosauropods, testing the existence of diverging patterns between (evolutionary level) and within (ontogenetic level) macronarian and diplodocoid species, relying on size series separated at reasonably low taxonomic level, that the numerous remains collected in the Morrison Formation (Tschopp et al. 2022) can provide.

Part 4: Morphofunctional implications for locomotion and weight-bearing

4.1 To which extent can we make comparisons with heavy mammals?

Contrary to heavy mammals (Gregory 1912, Osborn 1929, Etienne et al. 2020), the proximal half of the astragalus does not appear flatter in larger sauropodomorphs, whereas the distal articular surface is congruently flatter when size increases (fig. 5B). Such contrasting results might first appear counter-intuitive, but were in fact expectable as ankles function differently in mammals and dinosaurs. In the latter, the proximal part of the astragalus is anchored to the tibia, and mobility occurs on the astragalar distal roller. Therefore, although contacting surfaces may be reduced (particularly in sauropods, with reduction of the tibial descending process, see Lefebvre et al. 2022),

1003 the tibia connects more tightly to a more concave medial half and to more proximally developed
1004 processes on the posterior margin of the median ridge (Fig. 5B). Likewise, the fibular distal end is
1005 more tightly interlocked with the lateral face of the astragalus, as indicated by more marked
1006 outlines. This condition results in a more tightly connected astragalus acting analogously to the
1007 distal hindlimb zeugopod of heavy mammals. Distally, the flattening of the distal roller is consistent
1008 with the tendency observed in the distal crus of heavy mammals such as rhinoceroses (Mallet et al.
1009 2019), although sauropods differ in having their peculiarly oriented articular surface. Although this
1010 orientation variation is difficult to precisely quantify (see section 1.1), one cannot ignore that
1011 sauropod astragalar distal rollers are objectively more anteriorly oriented than those of non-
1012 sauropod sauropodomorphs (Fig. 4B), resulting in a more horizontal orientation of metatarsals
1013 (Bonnan 2005, see notably fig. 16.6). This pose was proposed as a feature playing a role in
1014 preserving a powerful capacity for plantarflexors (notably the *gastrocnemius*) that probably played
1015 a significant role in propulsion during locomotion (Bonnan 2005), while heavy mammals such as
1016 elephants were interpreted as keeping a vertical organisation of the metatarsals (Bonnan 2005). We
1017 corroborate the interpretation that a more anterior angulation of the distal roller acted as maintaining
1018 a sharp angle for the *gastrocnemius* insertion in columnar-limbed sauropods (Bonnan 2005, fig.
1019 16.6C, see a reconstitution in *e.g.* Borsuk-Bialynicka 1977, fig. 17B) that would have been lost with
1020 the loss of the flexed position of the hindlimb as seen in non-sauropodan sauropodomorphs
1021 (Bonnan 2005, fig. 16.6A, see a reconstitution in *e.g.* Langer 2003, fig. 8A). This constrain does not
1022 apply to columnar mammals, such as elephants and the rhinocerotoid *Paraceratherium*, as they
1023 possess a developed *tuber calcanei* where plantarflexors insert (Bonnan 2005; Etienne et al. 2020,
1024 see notably fig. 16). Current understanding of pes evolution in proboscideans also implies increase
1025 in metatarsal uprising departing from a plesiomorphically truly plantigrade condition (Hutchinson et
1026 al. 2011). Moreover, the astragalus in elephants shows smoother angulation of their proximal and
1027 distal articular surfaces (Osborn 1929, see notably fig. 665), which is thought to result in an almost
1028 vertical transfer of force from the hindlimb zeugopod to the distal autopod, similarly to rhinoceroses

(Osborn 1929, Etienne et al. 2020). However, the standardization of this observation (Osborn 1929, fig. 665) does not account for the anatomical orientation of the astragalus in elephants, that is, with the tibial facet proximally oriented, beneath a more vertically-oriented tibia, as well as an anteriorly projected navicular facet, resulting in more anteriorly projecting metatarsals (see *e.g.* Weissengruber et al. 2006, fig. 4 and Hutchinson et al. 2011, fig. 3). This contrasts with the more upright position of the metatarsals in extant rhinoceroses (see von Houwald 2001, Dudley et al. 2015, Etienne et al. 2024) and in the columnar *Paraceratherium* (Granger et al. 1936, fig. 42), congruently with astragalar angulation (Etienne et al. 2020). Also, pes architecture is not static and varies depending on loading (Hutchinson et al. 2011). Interestingly, the elephant pes is more horizontally oriented than the manus, and this condition is extremal under high loading (Hutchinson et al. 2011, see notably fig. 3).

In essence, both elephants and eusauropods share a more horizontal pes organisation compared to other sauropodomorphs and other heavy mammals, respectively; and both possess a distally extensive foot pad. In light of this correlation, we may hypothesize a causal link between those two features, so that the evolution of such an extensive pad requires a (sub)horizontal pes organisation allowing to achieve functional plantigrady. Such a pad is, potentially, only possible when metatarsals and phalanges are also very short or reduced, as seen in both groups (Osborn 1929, Wilson & Sereno 1998, Wilson 2005). Functionally, having a soft foot pad directly beneath the tarsus, while having horizontally deflected digits may alleviate loading pressure on the latter, resulting in greatly reducing biomechanical stresses induced by weight-bearing, congruently with conclusions made by a recent biomechanical study (Jannel et al. 2022). But such pad probably also imply less control of the loading pressure, as soft tissues composing it are more easily deformed by loading. Hutchinson et al. (2011) highlighted that the stiffness of the foot pad is ensured by the presence of predigits (“sixth-toe”) in elephants. They also hypothesized that pad expansion was rather limited in rhinos and hippos because of their lack of such predigits, and/or reduction/loss of first digit. It is, however, unclear if (eu)sauropods had similar structures. Perhaps the lack of

expansion in rhinos and hippos is also related to a more upright autopodial architecture, with elongated metapods, that is probably not compatible with the extension of the pad distally beneath the ankle.

4.2 Interplay with evolutionary innovations in the sauropod bauplan

If our interpretation is relevant and biologically meaningful, the analogous condition of eusauropods and elephants would have raised from very different evolutionary pathways. Eusauropod pes would have derived from a more upright and digitigrade ancestral morphotype, with subvertical metatarsals, similar to the condition seen in early bipedal sauropodomorphs. Contrastingly, the pes of elephants derived from a truly plantigrade ancestral morphotype, with horizontal metatarsals (Hutchinson et al. 2011). Those converging trajectories probably relate to totally different selective pressures, *i.e.* relating to the evolution of obligate quadrupedality in plesiomorphically bipedal sauropodomorphs, and increasing dominance of terrestrial ecologies in already plesiomorphically quadrupedal proboscideans (Hutchinson et al. 2011). In both cases, though, the peculiar pedal condition is preceded or concomitant with the evolution of a columnar architecture of the limb, which led to the evolution of extreme gigantism.

In sauropods, the “fully” functionally plantigrade foot pad was certainly shared by all eusauropods (Wilson 2005, Lallensack et al. 2017), but the exact condition seen in non-eusauropod taxa remains still unclear (Jannel et al. 2019, 2022), although early sauropods such as *Tazoudasaurus* are usually believed to lack such structure because of their relatively elongated metatarsals (Wilson 2005, Lallensack et al. 2017). Recently, a biomechanical analysis corroborated that the “fully” functionally plantigrade pad was critical for eusauropods to bear their weight, but also suggested that pad structures were essential even in non-sauropodan sauropodomorphs such as *Plateosaurus*, perhaps having a more restricted pad structure (see Jannel et al. 2022), to some extent similarly to large extant terrestrial birds (see Jannel et al. 2019). The particular condition of *Tazoudasaurus’* astragalus (section 1.2), associated with rather elongated metatarsals (*i.e.* similar to the elongated

condition of non-sauropodan sauropodomorphs) advocates for the idea that the evolution of a "fully" distally extended fleshy pad is partly decorrelated (*i.e.*, non-concomitant) from the acquisition of columnarity, and is acquired subsequently in eusauropods. However, Lallensack et al. (2017) described tracks with a possible extensive foot pad in the Late Triassic of Greenland. This might indicate that eusauropods' origin was much earlier than is suggested by our knowledge of the bony fossil record, or might correspond to independent evolution of the feature in a closely-related lineage (Wilson 2005, Lallensack et al. 2017). On a larger scale, our results match inferences made about the evolutionary modalities related to the evolution of the hindlimb long bones in sauropodomorphs, i.e., showing a more stepwise acquisition of features related to the evolution of the sauropod bauplan, comparatively to the forelimb ones whose evolution was more abrupt (Lefebvre et al. 2022). This is particularly true considering the evolutionary pattern seen for the tibia and the fibula, whose variations does not exclusively coincide with columnarity (although allometric patterns show less concordance, see section 3.2). Morphological traits show finer-level variation within columnar taxa that certainly correspond to more subtle within-clade specialisation among eusauropods.

At the level of the whole skeleton, the distribution of morphological diversity highlighted in part 2.1 tends to separate the diplodocoids (including "*Barosaurus africanus*") from a group constituted by brachiosaurids and non-neosauropod eusauropods. Such partitioning correlates with the evolution of the axial skeleton recently hypothesized by Vidal et al. (2020) who, by virtually mounting a skeletal model of *Spinophorosaurus*, highlighted that its wedged sacrum was probably a specialisation to high-browsing foraging, which was likely a synapomorphy of eusauropods. This condition is indeed shared by all analysed taxa, and low-browsing species, notably diplodocoids, had counteracting features such as shorter forelimbs and obtuse dorsal vertebrae, while taxa such as brachiosaurids exaggerated the ancestral foraging ecology with particularly long forelimbs. Likewise in our analysis, we highlight that brachiosaurids share morphological similarity with non-neosauropods (*Lapparentosaurus* and *Turisaurus* are indeed sharing more affinities with the C.2 than the C.1

morphotype from Fig. 7, see Appendix S1B), while sampled diplodocoids share a markedly different morphotype. Notably, diplodocoids also have apomorphic pedal proportions, as highlighted by Carrano (2005), as well as with some morphological peculiarities (*e.g.* relatively gracile tibia and fibula) highlighted for long bones for similar distributions of specimens by Lefebvre et al. (2022). Overall, this suggests that the general appendicular morphology characterizing diplodocoids does not mainly retain the plesiomorphic morphotype of eusauropods or even sauropods, as often thought (*e.g.* Carrano 2005), and in fact shows a suite of numerous derived features.

4.3 What remains unknown: the probable role of cartilage

Main features highlighted in our study may not have obvious functional implications, but they reflect differing ossification patterns especially within sauropods.

For instance, diplodocoid astragalus appear less elongated medially relatively (especially) to brachiosaurids, while they usually show larger development of the distal swelling of the lateral articular surface. This latter condition is perhaps related to the poor ossification of the calcaneum especially in diplodocoids, although this bone is also seldom found in taxa from other eusauropod clades (Bonnan 2000). Proportionately, the ossified astagalus also tends to not fully cover the articulating distal surface of the tibia, especially in macronarians such as in *Erketu* (Ksepka & Norell 2006), *Euhelopus* (Wilson & Upchurch 2009), *Gobititan* (You et al. 2003) and *Opisthocoelicaudia* (Borsuk-Bialynicka 1977). Beyond this diversity of patterns, a trend to a decrease of tarsal ossification is discernible along sauropod evolutionary history, compared to non-sauropodan sauropodomorphs that retain complete covering of the distal tibia by ossified astragalus and presence of at least some ossified distal tarsals (see *e.g. Mussaurus* in Otero & Pol 2013 and *Blikanasaurus* in Galton & von Heerden 1998). This strongly suggests a diminishing contribution of ossification in the sauropod ankle, likely in favour of a greater proportion of cartilage. Indeed, as in most non-mammalian and non-lepidosaur tetrapods, sauropodomorphs retained cartilaginous

epiphyses that may have accounted for up to 10% of the total limb bone length (Holliday et al. 2010; see also Bonnan et al. 2010 and Voegele et al. 2022) that are thought to have provided more efficient shock absorption and weight support (Holliday et al. 2010, Bonnan et al. 2013, Tsai et al. 2020). This certainly also concerned the sauropod tarsal bones, that functionally acted as the distal extremity of the hindlimb zeugopod, so that an increasing proportion of cartilage likely contributed to the evolution of gigantic proportions in sauropod species.

Part 5: Can we confidently assess the tempo and mode of astragalar evolution in sauropodomorphs?

At best, our results suggest a shift towards lower rates of morphological evolution occurring in eusauropods. In this sense, our result can be interpreted to reflect a slow-down related to selective pressures stabilizing morphological evolution around an adaptive optimum (see Castiglione et al. 2018). Such an interpretation matches the rest of our analyses suggesting a marked distinction in eusauropods (see section 1), perhaps in relation with the evolution of an extensive foot pad (see section 4), as we may reasonably assume that astragalar shape is a key component in locomotion and weight-bearing (see intro). It could be also congruent with the analysis of dinosaur body mass of Castiglione et al. (2018) who linked the lower rates observed in sauropods to their quadrupedal mode of locomotion. This slow-down could have been a prerequisite to the extreme form of gigantism reached only within eusauropod in several independent subclades (Sander et al. 2011).

However, the pattern we found can find alternative explanations. An adaptive explanation of the relationship between astragalar morphology and its rate of evolution is very tempting, but could also be the consequence of trait covariation with another feature being alone under selective pressure (see Gould & Lewontin 1979). An explicit appraisal of the link between estimated performance (in locomotion and weight-bearing) and astragalar shape, by the means of a biomechanical analysis, is strongly desired to support more reliably inferences regarding any adaptive hypothesis.

Whatever the speculations we can make on the biological meaning of finding such a shift, our analysis revealed that inference of evolutionary rates were highly sensitive to temporal uncertainty. While at first no significant shift was detected using arbitrarily either the FAD or LAD topology (Fig. 4, table 1), our randomization procedure revealed that the opposite result was in fact recovered 51% of the time (Table 1). Additionally, this frequency was also sensitive to arbitrary choice of the minimal branch length value (Table 2), impacting internal branch reconstructions, with significant result found in more than 90% of cases, and with high variability in estimated values (Table 3). Given the sensitivity to uncertain temporal parameters, we cannot confidently favour any hypothesis regarding the presence or absence of a shift in evolutionary rates for astragalar shape. One may of course argue that our study sample was a small number of species with usually poor knowledge of their actual temporal distribution, but this caveat occurs very frequently for palaeobiological studies focused in studying continental vertebrate clades, only known by fossil species (often only known by one or few partial individuals). Specifically for sauropodomorphs, recent studies (e.g. Pol et al. 2020, 2021) relying on absolute datation and enriching our knowledge of Lower Jurassic faunas, hint at promising discoveries further documenting the faunal turnover occurring between eusauropod and non-eusauropod sauropodomorphs that is thought to have occurred between the Pliensbachian and the Toarcian (Allain & Aquesbi 2008, Pol et al. 2020). Further documentation of early taxa such as *Bagualia* (Pol et al. 2020), with better constrained stratigraphic occurrence for already described taxa, will help in better understanding how morphological evolution occurred in the sauropodomorph astragalus. Future discoveries will perhaps confirm ichnological studies suggesting a possible Triassic origin for eusauropods (Lallensack et al. 2017). In addition, a more integrative look at the other skeletal elements would help in providing support to any hypothesis. Congruent signal in forelimb and hindlimb long bones patterns (Lefebvre et al. 2022) indeed gave more support for surprising outcomes, such as differential patterns between bones and allometric trajectories.

More generally, our study strongly advocates to systematically explore sensitivity to temporal uncertainty. This applies when using, as in our case, a phylogenetic ridge regression to estimate evolutionary rates, but could concern virtually every phylogenetic comparative method, especially in cases including fossil taxa. In any case, we feel that it is important to correctly address the degree of confidence one could put on such analyses, testing each *ad hoc* assumption necessary to process the analysis, perhaps by establishing in the future standardized and easily executable protocols to do so. In the example of our study, restraining our analysis to FAD and/or LAD topologies would have led us to conclude for no support *at all* for a shift in evolutionary rates, while our randomization procedure permitted us to assess that a significant shift *might have been* possible.

Conclusion

Our extensive analysis of morphological evolution of the sauropodomorph astragalus highlighted clear distinction between columnar and non-columnar taxa. More precisely, our results are congruent with a stepwise acquisition of morphological features in relation to the emergence of sauropods, with its earlier representative, *Tazoudasaurus*, showing a mixture of traits found in either non-sauropodan sauropodomorphs or in eusauropods. Additionally, subtler variation also exists in eusauropods, with features discriminating for example brachiosaurids and diplodocoids, such as a particular anteromedially-projected apex in the former, and a developed distal swelling in the latter. In both cases, while some of those features are captured in phylogenetic studies aiming to disentangle the relationships of those dinosaurs, our study also highlighted morphological variations, such as the shape of the lateral articular surface and the relative proportions of posterior subfossae, that remained to our knowledge undocumented in matrices found in the literature, thereby leading us to suggest the creation or modification of several phylogenetic characters coded according to astragalar morphological variation. Non-sauropodan sauropodomorphs also showed variability perhaps linked to their apparent substantial phenotypic plasticity, with the existence of

two general morphs, a blocky and a more elongated one. In larger sauropodomorphs, size-related variations such as flattening of the distal articular surface was consistent with previous analyses of the tarsus in heavy mammals, while incongruent features such as the particular development of the proximal part were explained by the morphofunctional differences between those groups. This precise feature probably relates to tighter interlocking of the astragalus to the distal zeugopod, acting analogously to the distal crus of mammals. Functionally, the eusauropod astragalus is particularly interesting in having a more anteriorly directed distal articular surface, which correlates with the loss of the anterolateral triangular surface, whose absence appears as the most objective qualitative proxy of this peculiar subhorizontal orientation. Interestingly, a rather horizontal organization of the tarsus is also found to some extent in elephants, when compared to other heavy mammals such as rhinoceroses. This may be related to the evolution of a posteriorly extensive foot pad, only found in those two groups, although originating from clearly different evolutionary paths. This hypothesis at best *could be* supported by our analysis of evolutionary rates, highlighting that a shift towards lower rates *might have* occurred in or within eusauropods. However, our randomization procedure accounting for stratigraphic uncertainty showed that these results were highly sensitive to *ad hoc* temporal parametrizations (occurrence date of terminal taxa, minimal branch lengths). Beyond the specific topic of our study, our analyses strongly advocate for more explicit assessment of robustness of results to unknown parameters, resulting in better assessment of the degree of confidence one can put on interpretations of phylogenetically-informed palaeobiological studies.

Conflict of interest

The authors declare no conflict of interest.

Data Availability Statement

Most of the data that support the findings of this study are or will be made available in respective museum repositories and/or by curators, and unless otherwise decided, deposited in Morphosource.

Acknowledgments

We warmly thank Rafael Royo-Torres (Museo de la Fundación Conjunto Paleontológico de Teruel-Dinópolis [CPT], Teruel, Spain); You Hailu (Institute of Vertebrate Paleontology and Paleoanthropology, Beijing, China); Martin Ezcurra, Marcel Asciano, Guillermo Aguirrezabala and Emiliano Petter Lalia (Museo Argentino de Ciencias Naturales Bernardino Rivadavia [MACN], Buenos Aires, Argentina); Daniela Schwarz (Museum für Naturkunde [MB.R], Berlin, Germany); Musée des Dinosaures ([MDS], Savannakhet, Laos); Mohamed Ghamizi (Muséum d'Histoire naturelle [MHNM], Marrakesh, Morocco); Marcelo Reguero and Alejandro Otero (Museo de La Plata [MLP], La Plata, Argentina); Ronan Allain, Sandra Daillie, Damien Olivier, Vincent Pernègre & Renaud Vacant (Muséum National d'Histoire Naturelle [MNHN], Paris, France), Pablo Ortiz and Rodrigo González (Instituto Miguel Lillo, Universidad Nacional de Tucumán [PVL], San Miguel de Tucumán, Argentina), Ricardo Martínez, Cecilia Apaldetti and Diego Abelín (Instituto y Museo de Ciencias Naturales, Universidad Nacional de San Juan [PVSJ], San Juan, Argentina); Rainer Schoch (Staatliches Museum für Naturkunde [SMNS], Stuttgart, Germany) for providing access to the specimens. We would also like to thank Ronan Allain & Camille Bader (MNHN, Paris, France) for acquiring photogrammetric stacks respectively of MDS and SMNS specimens. We thank also Ronan Allain, Camille Bader, Raphaël Cornette, Cyril Etienne, Helder Gomes Rodrigues, Romain Pintore, (MNHN, Paris, France), Pauline Hanot (Institut des Sciences de l'Évolution de Montpellier, Montpellier, France) and Martin Segesdi (Eötvös Loránd University, Budapest, Hungary) for their helpful advises and constructive comments. We thank Paolo Piras (Università Roma Tre, Rome, Italy) & Pasquale Raia (Università di Napoli Federico II, Napoli, Italy) for providing help and access to their intercept test in R. We finally thank the anonymous reviewer and the editors, whose comments improved the content of this manuscript.

Authors contributions

Rémi Lefebvre and Alexandra Houssaye designed the study. Rémi Lefebvre, Chloé Aubry and Heinrich Mallison acquired the data. Rémi Lefebvre and Chloé Aubry performed the analyses. Rémi Lefebvre, Chloé Aubry and Alexandra Houssaye analyzed and interpreted the results. Rémi Lefebvre drafted the manuscript. All authors revised and approved the manuscript.

Funding

This work was funded by the European Research Council and is part of the GRAVIBONE project (ERC-2016-STG-715300)

1270 # References

Adams DC, Otárola-Castillo E. geomorph: an R package for the collection and analysis of geometric morphometric shape data, *Methods in ecology and evolution* 2013; **4**: 393–399.

Agisoft LLC. Photoscan Professional Edition 2018

Allain R, Aquesbi N. Anatomy and phylogenetic relationships of *Tazoudasaurus naimi* (Dinosauria, Sauropoda) from the late Early Jurassic of Morocco, *Geodiversitas* 2008; **30**: 345–424.

Allain R, Taquet P, Battail B *et al.* Un nouveau genre de dinosaure sauropode de la formation des Grès supérieurs (Aptien-Albien) du Laos, *Comptes Rendus de l'Académie des Sciences-Series IIA-Earth and Planetary Science* 1999; **329**: 609–616.

Angst D, Buffetaut E, Lecuyer C *et al.* A new method for estimating locomotion type in large ground birds, *Palaeontology* 2016; **59**: 217–223.

Apaldetti C, Martínez RN, Cerda IA *et al.* An early trend towards gigantism in Triassic sauropodomorph dinosaurs, *Nature ecology & evolution* 2018; **2**: 1227–1232.

Apaldetti C, Pol D, Yates A. The postcranial anatomy of Coloradisaurus brevis (Dinosauria: Sauropodomorpha) from the Late Triassic of Argentina and its phylogenetic implications, *Palaeontology* 2013; **56**: 277–301.

Artec 3D. Artec Studio Professional 2018

Bader C, Delapré A, Göhlich UB *et al.* Diversity of limb long bone morphology among proboscideans: how to be the biggest one in the family, *Papers in Palaeontology* 2024; **10**: e1597.

Bader C, Delapré A, Houssaye A. Shape variation in the limb long bones of modern elephants reveals adaptations to body mass and habitat, *Journal of Anatomy* 2023; **242**: 806–830.

Bajpai S, Datta D, Pandey P *et al.* Fossils of the oldest diplodocoid dinosaur suggest India was a major centre for neosauropod radiation, *Scientific Reports* 2023; **13**: 12680.

Baken EK, Collyer ML, Kaliontzopoulou A *et al.* geomorph v4. 0 and gmShiny: Enhanced analytics and a new graphical interface for a comprehensive morphometric experience, *Methods in Ecology and Evolution* 2021; **12**: 2355–2363.

Bapst DW. paleotree: an R package for paleontological and phylogenetic analyses of evolution, *Methods in Ecology and Evolution* 2012; **3**: 803–807.

Bell MA, Lloyd GT. strap: an R package for plotting phylogenies against stratigraphy and assessing their stratigraphic congruence, *Palaeontology* 2015; **58**: 379–389.

Biewener AA. Mammalian terrestrial locomotion and size, *Bioscience* 1989; **39**: 776–783.

Blanco MVF, Ezcurra MD, Bona P. New embryological and palaeontological evidence sheds light on the evolution of the archosauromorph ankle, *Scientific Reports* 2020; **10**: 5150.

Bonnan MF. The presence of a calcaneum in a diplodocid sauropod, *Journal of Vertebrate Paleontology* 2000; **20**: 317–323.

Bonnan MF. Pes anatomy in sauropod dinosaurs: implications for functional morphology, evolution, and phylogeny. In: Tidwell V, Carpenter K, eds. Thunder-Lizards: The Sauropodomorph Dinosaurs. Bloomington: Indiana University Press, 2005; 346–380.

Bonnan MF, Sandrik JL, Nishiwaki T *et al.* Calcified cartilage shape in archosaur long bones reflects overlying joint shape in stress-bearing elements: Implications for nonavian dinosaur locomotion, *The Anatomical Record: Advances in Integrative Anatomy and Evolutionary Biology* 2010; **293**: 2044–2055.

Bonnan MF, Wilhite DR, Masters SL *et al.* What lies beneath: sub-articular long bone shape scaling in eutherian mammals and saurischian dinosaurs suggests different locomotor adaptations for gigantism, *PloS one* 2013; **8**: e75216.

Borsuk-Bialynicka M. A new camarasaurid sauropod *Opisthocoelicaudia skarzynskii* gen. n., sp. n. from the Upper Cretaceous of Mongolia, *Palaeontologia Polonica* 1977; **37**: 5–64.

Botton-Divet L, Cornette R, Fabre AC *et al.* Morphological analysis of long bones in semi-aquatic mustelids and their terrestrial relatives, *Integrative and comparative biology* 2016; **56**: 1298–1309.

Brinkman D. The origin of the crocodiloid tarsi and the interrelationships of thecodontian archosaurs, *Brevoria* 1981; **464**: 1–23.

Carballido JL, Pol D, Otero A *et al.* A new giant titanosaur sheds light on body mass evolution among sauropod dinosaurs, *Proceedings of the Royal Society B: Biological Sciences* 2017; **284**: 20171219.

Carrano M. What, if anything, is a cursor? Categories versus continua for determining locomotor habit in mammals and dinosaurs, *Journal of Zoology* 1999; **247**: 29–42.

Carrano MT. The evolution of sauropod locomotion: morphological diversity of a secondarily quadrupedal radiation. In: Curry Rogers K, Wilson J, eds. The sauropods: evolution and paleobiology. Berkeley: University of California Press, 2005; 229–249.

Cashmore DD, Mannion PD, Upchurch P *et al.* Ten more years of discovery: revisiting the quality of the sauropodomorph dinosaur fossil record, *Palaeontology* 2020;: 1–28.

Castiglione S, Tesone G, Piccolo M *et al.* A new method for testing evolutionary rate variation and shifts in phenotypic evolution, *Methods in Ecology and Evolution* 2018; **9**: 974–983.

Cerda IA, Pol D, Otero A *et al.* Palaeobiology of the early sauropodomorph Mussaurus patagonicus inferred from its long bone histology, *Palaeontology* 2022; **65**: e12614.

Chapelle KE, Botha J, Choiniere JN. Extreme growth plasticity in the early branching sauropodomorph Massospondylus carinatus, *Biology Letters* 2021; **17**: 20200843.

Christiansen P. Locomotion in sauropod dinosaurs, *Gaia* 1997; **14**: 45–75.

Cignoni P, Callieri M, Corsini M *et al.* Meshlab: an open-source mesh processing tool. Eurographics Italian chapter conference. 2008; 129–136.

Coombs WP. Theoretical aspects of cursorial adaptations in dinosaurs, *The Quarterly Review of Biology* 1978; **53**: 393–418.

Cooper MR. The prosauropod dinosaur *Massospondylus carinatus* Owen from Zimbabwe: its biology, mode of life and phylogenetic significance., *Occasional Papers of the National Museums and Monuments, rhodesia, Series B, Natural Sciences* 1981; **6**: 689–840.

Cooper MR. A reassessment of *Vulcanodon karibaensis* Raath (Dinosauria: Saurischia) and the origin of the Sauropoda, *Palaeontogia africana* 1984; **25**: 203–231.

Dai H, Tan C, Xiong C *et al.* New macronarian from the Middle Jurassic of Chongqing, China: phylogenetic and biogeographic implications for neosauropod dinosaur evolution, *Royal Society Open Science* 2022; **9**: 220794.

D'Emic M. The early evolution of titanosauriform sauropod dinosaurs, *Zoological Journal of the Linnean Society* 2012; **166**: 624–671.

Dudley RJ, Wood SP, Hutchinson JR *et al.* Radiographic protocol and normal anatomy of the hind feet in the white rhinoceros (Ceratotherium simum), *Veterinary Radiology & Ultrasound* 2015; **56**: 124–132.

Esquerré D, Sherratt E, Keogh JS. Evolution of extreme ontogenetic allometric diversity and heterochrony in pythons, a clade of giant and dwarf snakes, *Evolution* 2017; **71**: 2829–2844.

Etienne C, Houssaye A, Fagan MJ *et al.* Estimation of the forces exerted on the limb long bones of a white rhinoceros (Ceratotherium simum) using musculoskeletal modelling and simulation, *Journal of Anatomy* 2024; **240**: 245–257.

Etienne C, Mallet C, Cornette R *et al.* Influence of mass on tarsus shape variation: a morphometrical investigation among Rhinocerotidae (Mammalia: Perissodactyla), *Biological Journal of the Linnean Society* 2020; **129**: 950–974.

Fau M, Cornette R, Houssaye A. Photogrammetry for 3D digitizing bones of mounted skeletons: potential and limits, *Comptes Rendus Palevol* 2016; **15**: 968–977.

Ferreira-Cardoso S, Billet G, Gaubert P *et al.* Skull shape variation in extant pangolins (Pholidota: Manidae): allometric patterns and systematic implications, *Zoological Journal of the Linnean Society* 2020; **188**: 255–275.

Gallina PA, Apesteguía S, Carballido JL *et al.* Southernmost Spiny Backs and Whiplash Tails: Flagellicaudatans from South America. South American Sauropodomorph Dinosaurs: Record, Diversity and Evolution. Springer, 2022; 209–236.

Galton PM, van Heerden J. Anatomy of the prosauropod dinosaur Blikanasaurus cromptoni (Upper Triassic, South Africa), with notes on the other tetrapods from the lower Elliot Formation, *Paläontologische Zeitschrift* 1998; **72**: 163–177.

Gilmore CW. Osteology of Apatosaurus, with species reference to specimens in the Carnegie Museum. Carnegie Institute, 1936.

Goodall C. Procrustes methods in the statistical analysis of shape, *Journal of the Royal Statistical Society: Series B (Methodological)* 1991; **53**: 285–321.

Gould SJ, Lewontin RC. The spandrels of San Marco and the Panglossian paradigm: a critique of the adaptationist programme, *Proceedings of the royal society of London. Series B. Biological Sciences* 1979; **205**: 581–598.

Gower JC. Generalized procrustes analysis, *Psychometrika* 1975; **40**: 33–51.

Granger W, Gregory WK, Osborn HF. Further notes on the gigantic extinct rhinoceros, Baluchitherium, from the Oligocene of Mongolia., *Bulletin of the AMNH* 1936; **72**.

Gregory WK. Notes on the principles of quadrupedal locomotion and on the mechanism of the limbs in hoofed animals, *Annals of the New York Academy of Sciences* 1912; **22**: 267–292.

Gunz P, Mitteroecker P. Semilandmarks: a method for quantifying curves and surfaces, *Hystrix, the Italian Journal of Mammalogy* 2013; **24**: 103–109.

Gunz P, Mitteroecker P, Bookstein FL. Semilandmarks in three dimensions. In: Slice D, ed. Modern morphometrics in physical anthropology. New York: Kluwer Academic Publishers/Plenum Publishers, 2005; 73–98.

Hatcher JB. Diplodocus (Marsh): its osteology, taxonomy, and probable habits, with a restoration of the skeleton, *Memoirs of the Carnegie Museum* 1901; **1**: 1–63.

Hedrick BP, Dodson P. Lujiatun psittacosaurids: understanding individual and taphonomic variation using 3D geometric morphometrics, *PLoS One* 2013; **8**: e69265.

Henderson DM. Burly gaits: centers of mass, stability, and the trackways of sauropod dinosaurs, *Journal of Vertebrate Paleontology* 2006; **26**: 907–921.

Hildebrand M. Analysis of vertebrate structure. New York: John Wiley & Sons, 1982.

Holliday CM, Ridgely RC, Sedlmayr JC *et al.* Cartilaginous epiphyses in extant archosaurs and their implications for reconstructing limb function in dinosaurs, *PLoS One* 2010; **5**: e13120.

Holwerda FM, Pol D. Phylogenetic analysis of Gondwanan basal eusauropods from the Early-Middle Jurassic of Patagonia, Argentina, *Spanish Journal of Palaeontology* 2018; **33**: 289–298.

Houssaye A, Waskow K, Hayashi S *et al.* Biomechanical evolution of solid bones in large animals: a microanatomical investigation, *Biological Journal of the Linnean Society* 2016; **117**: 350–371.

von Houwald FF. Foot problems in Indian rhinoceroses (Rhinoceros unicornis) in zoological gardens: macroscopic and microscopic anatomy, pathology, and evaluation of the causes, 2001;

von Huene F. Vollstfindige Osteologie eines Plateosauriden aus dem schwfibischen Keuper., *GEOLOGISCHE UND PALBONTOLOGISCHE ABHANDLUNGEN* 1926; **15**: 1–43.

Hutchinson JR. The evolutionary biomechanics of locomotor function in giant land animals, *Journal of Experimental Biology* 2021; **224**: 217463.

Hutchinson JR, Delmer C, Miller CE *et al.* From flat foot to fat foot: structure, ontogeny, function, and evolution of elephant “sixth toes”, *Science* 2011; **334**: 1699–1703.

Janensch W. Die gliedmaßen und gliedmaßengürtel der Sauropoden der Tendaguru-Schichten, *Palaeontographica-Supplementbände* 1961;: 177–235.

Jannel A, Nair JP, Panagiotopoulou O *et al.* “Keep your feet on the ground”: Simulated range of motion and hind foot posture of the Middle Jurassic sauropod *Rhoetosaurus brownei* and its implications for sauropod biology, *Journal of morphology* 2019; **280**: 849–878.

Jannel A, Salisbury SW, Panagiotopoulou O. Softening the steps to gigantism in sauropod dinosaurs through the evolution of a pedal pad, *Science Advances* 2022; **8**: eabm8280.

Klein N, Sander PM. Bone histology and growth of the prosauropod dinosaur *Plateosaurus engelhardti* von Meyer, 1837 from the Norian bonebeds of Trossingen (Germany) and Frick (Switzerland), *Special Papers in Palaeontology* 2007; **77**: 169.

Klingenberg CP. Size, shape, and form: concepts of allometry in geometric morphometrics, *Development genes and evolution* 2016; **226**: 113–137.

Ksepka DT, Norell MA. Erketu ellisoni, a long-necked sauropod from Bor Guvé (Dornogov Aimag, Mongolia), *American Museum Novitates* 2006; **2006**: 1–16.

Lallensack JN, Klein H, Milàn J *et al.* Sauropodomorph dinosaur trackways from the Fleming Fjord Formation of East Greenland: evidence for Late Triassic sauropods, *Acta Palaeontologica Polonica* 2017; **62**: 833–843.

Läng E, Mahammed F. New anatomical data and phylogenetic relationships of Chebsaurus algeriensis (Dinosauria, Sauropoda) from the Middle Jurassic of Algeria, *Historical Biology* 2010; **22**: 142–164.

Langer MC. The pelvic and hind limb anatomy of the stem-sauropodomorph *Saturnalia tupiniquim* (Late Triassic, Brazil), *PaleoBios* 2003; **23**: 1–30.

Langer MC, Marsola JC, Müller RT *et al.* The early radiation of sauropodomorphs in the Carnian (Late Triassic) of South America. South American Sauropodomorph Dinosaurs: Record, Diversity and Evolution. Springer, 2022; 1–49.

Langer MC, Ramezani J, Da Rosa ÁA. U-Pb age constraints on dinosaur rise from south Brazil, *Gondwana Research* 2018; **57**: 133–140.

Lefebvre R, Allain R, Houssaye A. What’s inside a sauropod limb? First three-dimensional investigation of the limb long bone microanatomy of a sauropod dinosaur, Nigersaurus

taqueti (Neosauropoda, Rebbachisauridae), and implications for the weight-bearing function, *Palaeontology* 2023; **66**: e12670.

Lefebvre R, Allain R, Houssaye A *et al.* Disentangling biological variability and taphonomy: shape analysis of the limb long bones of the sauropodomorph dinosaur *Plateosaurus*, *PeerJ* 2020; **8**: e9359.

Lefebvre R, Houssaye A, Mallison H *et al.* A path to gigantism: Three-dimensional study of the sauropodomorph limb long bone shape variation in the context of the emergence of the sauropod bauplan, *Journal of Anatomy* 2022;

Mallet C, Billet G, Cornette R *et al.* Adaptation to graviportality in Rhinocerotoidea? An investigation through the long bone shape variation in their hindlimb, *Zoological Journal of the Linnean Society* 2022; **196**: 1235–1271.

Mallet C, Cornette R, Billet G *et al.* Interspecific variation in the limb long bones among modern rhinoceroses—extent and drivers, *PeerJ* 2019; **7**: e7647.

Mallison H. Rearing giants: kinetic-dynamic modeling of sauropod bipedal and tripodal poses, *Biology of the sauropod dinosaurs: Understanding the life of giants* 2011; **237**: 250.

Mallison H, Wings O. Photogrammetry in paleontology–a practical guide, *Journal of Paleontological Techniques* 2014; **12**: 1–31.

Mannion PD, Allain R, Moine O. The earliest known titanosauriform sauropod dinosaur and the evolution of Brachiosauridae, *PeerJ* 2017; **5**: e3217.

Mannion PD, Otero A. A reappraisal of the Late Cretaceous Argentinean sauropod dinosaur Argyrosaurus superbus, with a description of a new titanosaur genus, *Journal of Vertebrate Paleontology* 2012; **32**: 614–638.

Mannion PD, Upchurch P, Barnes RN *et al.* Osteology of the Late Jurassic Portuguese sauropod dinosaur Lusotitan atalaiensis (Macronaria) and the evolutionary history of basal titanosauriforms, *Zoological Journal of the Linnean Society* 2013; **168**: 98–206.

Mannion PD, Upchurch P, Schwarz D *et al.* Taxonomic affinities of the putative titanosaurs from the Late Jurassic Tendaguru Formation of Tanzania: phylogenetic and biogeographic implications for eusauropod dinosaur evolution, *Zoological Journal of the Linnean Society* 2019; **185**: 784–909.

Martinez RN, Alcober OA. A basal sauropodomorph (Dinosauria: Saurischia) from the Ischigualasto Formation (Triassic, Carnian) and the early evolution of Sauropodomorpha, *PLoS One* 2009; **4**: e4397.

McPhee BW, Benson RB, Botha-Brink J *et al.* A giant dinosaur from the earliest Jurassic of South Africa and the transition to quadrupedality in early sauropodomorphs, *Current Biology* 2018; **28**: 3143–3151.

Mitteroecker P, Gunz P. Advances in geometric morphometrics, *Evolutionary Biology* 2009; **36**: 235–247.

Mitteroecker P, Gunz P, Bernhard M *et al.* Comparison of cranial ontogenetic trajectories among great apes and humans, *Journal of Human Evolution* 2004; **46**: 679–698.

Müller RT. Astragalar anatomy of an early dinosaur from the Upper Triassic of southern Brazil, *Historical Biology* 2021; **33**: 2534–2541.

Novas FE. The tibia and tarsus in Herrerasauridae (Dinosauria, incertae sedis) and the origin and evolution of the dinosaurian tarsus, *Journal of Paleontology* 1989; **63**: 677–690.

O'Keefe FR, Sidor CA, Larsson HC *et al.* Evolution and homology of the astragalus in early amniotes: new fossils, new perspectives, *Journal of Morphology* 2006; **267**: 415–425.

Osborn HF. The titanotheres of ancient Wyoming, Dakota, and Nebraska. Washington, D.C.: Government Printing Office, 1929.

Ossa-Fuentes L, Mpodozis J, Vargas AO. Bird embryos uncover homology and evolution of the dinosaur ankle, *Nature Communications* 2015; **6**: 8902.

Otero A, Cuff AR, Allen V *et al.* Ontogenetic changes in the body plan of the sauropodomorph dinosaur Mussaurus patagonicus reveal shifts of locomotor stance during growth, *Scientific reports* 2019; **9**: 1–10.

Otero A, Peyre de Fabrègues C. Non-sauropodiform Plateosaurians: Milestones Through the "Prosauropod" Bauplan. South American Sauropodomorph Dinosaurs: Record, Diversity and Evolution. Springer, 2022; 51–92.

Otero A, Pol D. Postcranial anatomy and phylogenetic relationships of *Mussaurus patagonicus* (Dinosauria, Sauropodomorpha), *Journal of Vertebrate Paleontology* 2013; **33**: 1138–1168.

Pérez-Moreno A, Salgado L, Carballido JL *et al.* A new titanosaur from the La Colonia Formation (Campanian-Maastrichtian), Chubut Province, Argentina, *Historical Biology* 2024;: 1–20.

Peyre de Fabrègues C, Allain R. *Kholumolumo ellenbergerorum*, gen. et sp. nov., a new early sauropodomorph from the lower Elliot Formation (Upper Triassic) of Maphutseng, Lesotho, *Journal of Vertebrate Paleontology* 2020; **39**: e1732996.

Piras P, Salvi D, Ferrara G *et al.* The role of post-natal ontogeny in the evolution of phenotypic diversity in *Podarcis* lizards, *Journal of Evolutionary Biology* 2011; **24**: 2705–2720.

Pol D, Garrido A, Cerda IA. A new sauropodomorph dinosaur from the Early Jurassic of Patagonia and the origin and evolution of the sauropod-type sacrum, *PLoS One* 2011; **6**: e14572.

Pol D, Mancuso AC, Smith RM *et al.* Earliest evidence of herd-living and age segregation amongst dinosaurs, *Scientific reports* 2021; **11**: 20023.

Pol D, Ramezani J, Gomez K *et al.* Extinction of herbivorous dinosaurs linked to Early Jurassic global warming event, *Proceedings of the Royal Society B* 2020; **287**: 20202310.

Polly PD. Limbs in mammalian evolution. In: Hall B, ed. Fins into limbs: evolution, development and transformation. Chicago: University of Chicago Press Books, 2007; 245–268.

R Core Team. R: A language and environment for statistical computing. R Foundation for Statistical Computing; version 3.5.1 2018;

Rauhut O, Fechner R, Remes K *et al.* How to get big in the Mesozoic: the evolution of the sauropodomorph body plan. In: Klein N, Remes K, Gee CT, Sander PM, eds. Biology of the sauropod dinosaurs: Understanding the life of giants. Bloomington: Indiana University Press, 2011; 119–149.

Remes K. Taxonomy of Late Jurassic diplodocid sauropods from Tendaguru (Tanzania), *Fossil Record* 2009; **12**: 23–46.

Rohlf FJ, Slice D. Extensions of the Procrustes method for the optimal superimposition of landmarks, *Systematic Biology* 1990; **39**: 40–59.

Royo-Torres R, Cobos A, Alcalá L. A giant European dinosaur and a new sauropod clade, *Science* 2006; **314**: 1925–1927.

Royo-Torres R, Cobos A, Mocho P *et al.* Origin and evolution of turiasaur dinosaurs set by means of a new ‘rosetta’specimen from Spain, *Zoological Journal of the Linnean Society* 2021; **191**: 201–227.

Royo-Torres R, Upchurch P, Kirkland JI *et al.* Descendants of the Jurassic turiasaurs from Iberia found refuge in the Early Cretaceous of western USA, *Scientific Reports* 2017; **7**: 1–12.

Saitou N, Nei M. The neighbor-joining method: a new method for reconstructing phylogenetic trees, *Molecular biology and evolution* 1987; **4**: 406–425.

Salgado L, Coria RA, Calvo JO. Evolution of titanosaurid sauropods: Phytogenetic analysis based on the postcranial evidence., *Ameghiniana* 1997; **34**: 3–32.

Sander PM, Christian A, Clauss M *et al.* Biology of the sauropod dinosaurs: the evolution of gigantism, *Biological Reviews* 2011; **86**: 117–155.

Sander PM, Clauss M. Sauropod gigantism, *Science* 2008; **322**: 200–201.

Sander PM, Klein N. Developmental plasticity in the life history of a prosauropod dinosaur, *Science* 2005; **310**: 1800–1802.

Schlager S. Morpho and Rvcg–Shape Analysis in R: R-Packages for geometric morphometrics, shape analysis and surface manipulations. In: Zheng G, Li S, Szekely G, eds. Statistical shape and deformation analysis. Cambridge: Academic Press, 2017; 217–256.

Tsai HP, Middleton KM, Hutchinson JR *et al.* More than one way to be a giant: Convergence and disparity in the hip joints of saurischian dinosaurs, *Evolution* 2020; **74**: 1654–1681.

Tschopp E, Mateus O. Osteology of Galeamopus pabsti sp. nov.(Sauropoda: Diplodocidae), with implications for neurocentral closure timing, and the cervico-dorsal transition in diplodocids, *PeerJ* 2017; **5**: e3179.

Tschopp E, Mateus O, Benson RB. A specimen-level phylogenetic analysis and taxonomic revision of Diplodocidae (Dinosauria, Sauropoda), *PeerJ* 2015a; **3**: e857.

Tschopp E, Whitlock JA, Woodruff DC *et al.* The Morrison Formation Sauropod Consensus: A freely accessible online spreadsheet of collected sauropod specimens, their housing institutions, contents, references, localities, and other potentially useful information, *Peer Community Journal* 2022; **2**.

Tschopp E, Wings O, Hannover L *et al.* Articulated bone sets of manus and pedes of Camarasaurus (Sauropoda, Dinosauria), 2015b;.

Turner ML, Gatesy SM. Inner workings of the alligator ankle reveal the mechanistic origins of archosaur locomotor diversity, *Journal of Anatomy* 2023; **242**: 592–606.

Upchurch P, Barrett PM, Galton PM. A phylogenetic analysis of basal sauropodomorph relationships: implications for the origin of sauropod dinosaurs, *Special Papers in Palaeontology* 2007; **77**: 57–90.

Vidal D, Mocho P, Aberasturi A *et al.* High browsing skeletal adaptations in *Spinophorosaurus* reveal an evolutionary innovation in sauropod dinosaurs, *Scientific reports* 2020; **10**: 1–10.

Viglietti PA, Barrett PM, Broderick TJ *et al.* Stratigraphy of the Vulcanodon type locality and its implications for regional correlations within the Karoo Supergroup, *Journal of African Earth Sciences* 2018; **137**: 149–156.

Voegele KK, Siegler S, Bonnan MF *et al.* Constraining morphologies of soft tissues in extinct vertebrates using multibody dynamic simulations: a case study on articular cartilage of the sauropod Dreadnoughtus, *Frontiers in Earth Science* 2022;: 995.

Weissengruber G, Egger G, Hutchinson J *et al.* The structure of the cushions in the feet of African elephants (Loxodonta africana), *Journal of Anatomy* 2006; **209**: 781–792.

Whitlock JA. A phylogenetic analysis of Diplodocoidea (Saurischia: Sauropoda), *Zoological Journal of the Linnean Society* 2011; **161**: 872–915.

Wiley DF, Amenta N, Alcantara DA *et al.* Evolutionary morphing. Proceedings of IEEE visualization 2005. Piscataway: IEEE, 2005; 431–438.

Wilson JA. Sauropod dinosaur phylogeny: critique and cladistic analysis, *zoological Journal of the Linnean Society* 2002; **136**: 215–275.

Wilson JA. Integrating ichnofossil and body fossil records to estimate locomotor posture and spatiotemporal distribution of early sauropod dinosaurs: a stratocladistic approach, *Paleobiology* 2005; **31**: 400–423.

Wilson JA, Sereno PC. Early evolution and higher-level phylogeny of sauropod dinosaurs, *Journal of Vertebrate Paleontology* 1998; **18**: 1–79.

Wilson JA, Upchurch P. Redescription and reassessment of the phylogenetic affinities of Euhelopus zdanskyi (Dinosauria: Sauropoda) from the Early Cretaceous of China, *Journal of Systematic Palaeontology* 2009; **7**: 199–239.

Yates AM. The first complete skull of the Triassic dinosaur *Melanorosaurus* Haughton (Sauropodomorpha: Anchisauria), *Special Papers in Palaeontology* 2007;: 9–55.

You HL, Tang F, Luo Z. A new basal titanosaur (Dinosauria: Sauropoda) from the Early Cretaceous of China, *Acta Geologica Sinica-English Edition* 2003; **77**: 424–429.

Figures

Figure 1. Time-calibrated composite phylogeny of the sauropodomorph genuses sampled in our study. The taxa belonging to the clade Sauropoda (in red) are examined in this study compared to taxa belonging to non-sauropodiform sauropodomorphs (in green) and non-sauropodan sauropodiforms (in orange) grades. *Herrerasaurus* (in black) constitutes the outgroup. Subgroups recognizable within sauropods are numeroted from 1 to 5 (see on bottom right). Informal consensus based on Holwerda and Pol (2018) and Peyre de Fabrègues and Allain (2020) (see Material and Methods), using paleotree (Bapst, 2012) and strap (Bell & Lloyd, 2015) R packages. Silhouettes by Scott Hartman.

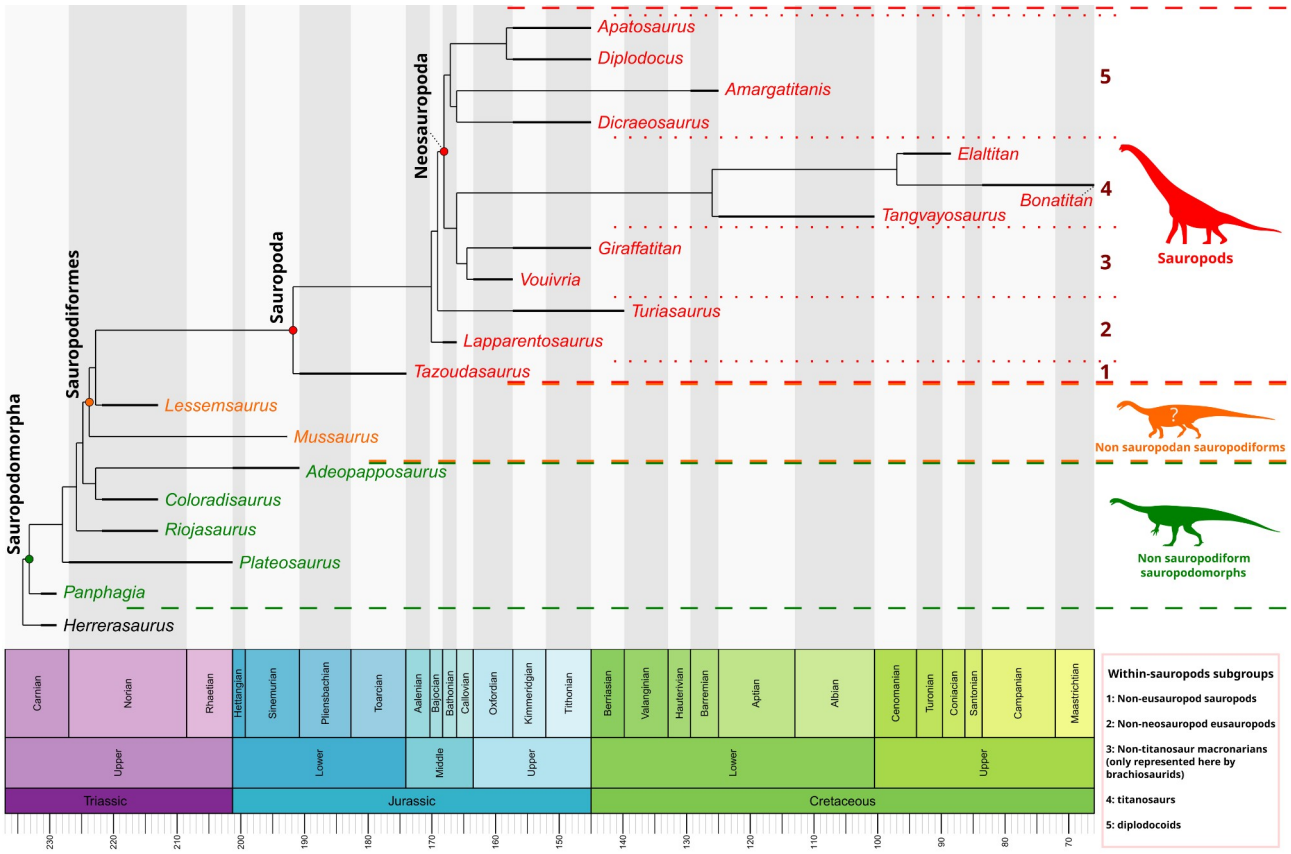

Figure 2. Morphological analysis of the sampling including titanosaurs. A, Neighbour Joining tree based on the euclidean distance matrix computed with the first ten principal components (PC) representing 90.03% of the total variation. Colours: Green: non-sauropodiform sauropodomorphs, orange: non-sauropodan sauropodiforms, red: sauropods, grey: outgroup (*Herrerasaurus*), blue: indeterminate. Taxonomic abbreviations: Ad: *Adeopapposaurus*; Am: *Amargatitanis*; Ap: *Apatosaurus*; Ba: "*Barosaurus africanus"*; Bo: *Bonatitan*; Co: *Coloradisaurus*; Dc: *Dicraeosaurus*; Dp: *Diplodocus*; El: *Elaltitan*; Gi: *Giraffatitan*; He: *Herrerasaurus*; La: *Lapparentosaurus*; Le: *Lessemsaurus*; Mu: *Mussaurus*; Pa: *Panphagia*; Pl: *Plateosaurus*; Ri: *Riojasaurus*; Ta: *Tazoudasaurus*; Tv: *Tangvayosaurus*; Vo: *Vouivria*. B, Morphospace analysis for the first two PCs. The diameter of the dots is proportional to specimens' centroid size. Colours: same as in A. The red convex hull represents space occupied by titanosaurs.

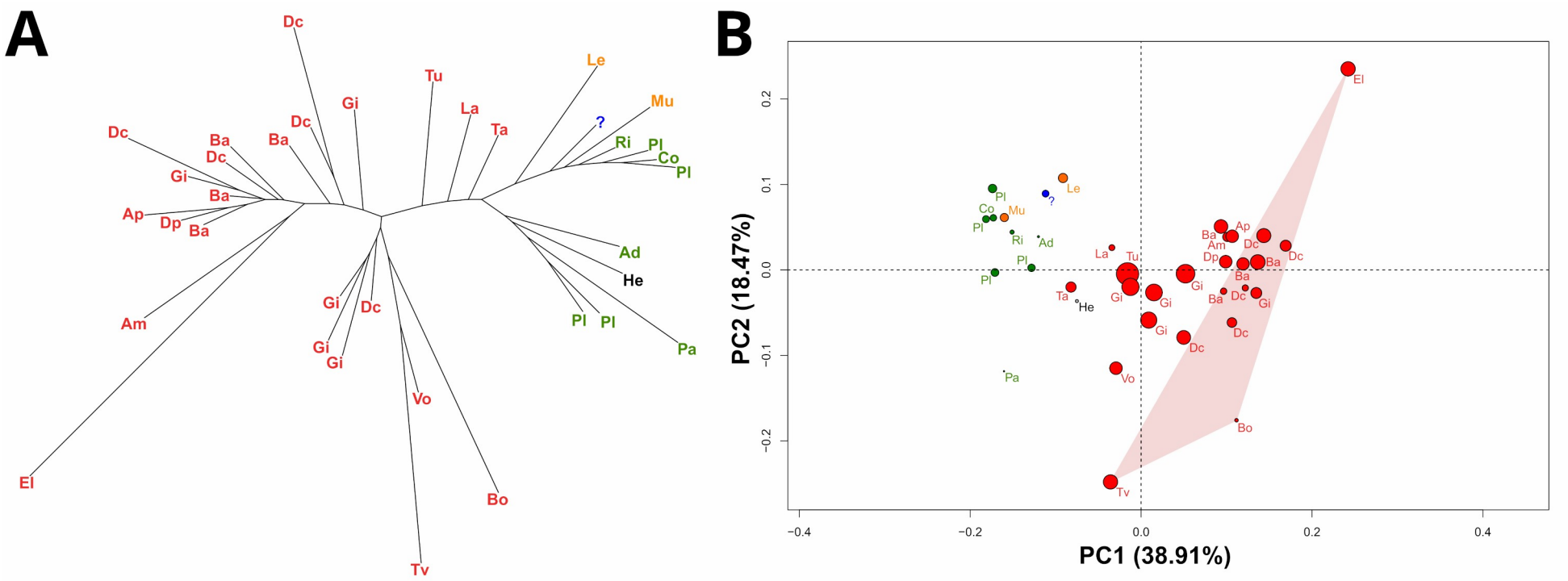
A
Dc
Le
Tu
Mu
Gi
La
?
Dc
Ta
Ri
Dc
Ba
Ba
Pl
Co
Dc
Pl
Gi
Ba
Ap
Dp
Ba
Ad
He
Am
Gi
Dc
Pl
Pl
Pa
Gi
Gi
Vo
El
Bo
Tv
B
El
Le
Pl
?
Co
Mu
Pl
Ri
Ad
Ba
Ap
Am
Dc
La
Tu
Dp
Dc
Pl
Ba
Ba
Pl
Gi
Ta
He
Gi
Gi
Ba
Dc
Gi
Gi
Dc
Dc
Pa
Vo
Bo
Tv
PC2 (18.47%)
PC1 (38.91%)
0.2
0.1
0.0
−0.1
−0.2
−0.4
−0.2
0.0
0.2
0.4

Figure 3. Neighbour Joining tree based on the euclidean distance matrix computed with the first eleven principal components representing 91.37% of the total variation. Colours: Green: non-sauropodiform sauropodomorphs, orange: non-sauropodan sauropodiforms, red: sauropods, grey: outgroup (*Herrerasaurus*). Taxonomic abbreviations: Ad: *Adeopapposaurus*; Am: *Amargatitanis*; Ap: *Apatosaurus*; Ba: *"Barosaurus africanus"*; Co: *Coloradisaurus*; Dc: *Dicraeosaurus*; Dp: *Diplodocus*; Gi: *Giraffatitan*; He: *Herrerasaurus*; La: *Lapparentosaurus*; Le: *Lessemsaurus*; Mu: *Mussaurus*; Pa: *Panphagia*; Pl: *Plateosaurus*; Ri: *Riojasaurus*; Ta: *Tazoudasaurus*; Vo: *Vouivria*.

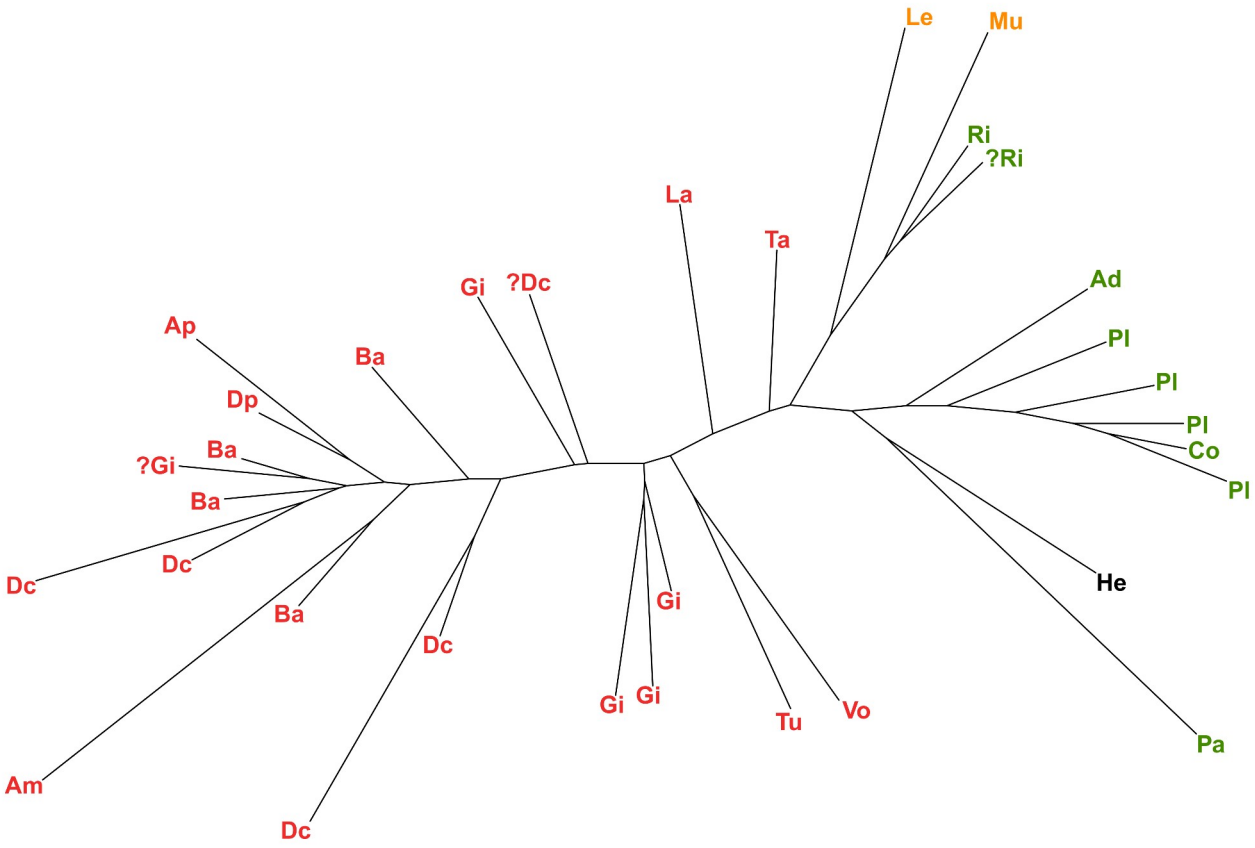

Figure 4. A, Phylomorphospace of the astragalus analysis along the first three principal components (PC). Green dots represent non-sauropodiform sauropodomorphs, orange dots represent non-sauropodan sauropodiforms, red dots represent sauropods, the grey dot represent the outgroup (*Herrerasaurus*). The diameter of the dots is proportional to specimens' centroid size. Node I corresponds to Sauropodomorpha, node II to Sauropodiformes, node III to Sauropoda, node IV to Neosauropoda. Taxonomic abbreviations: Ad: *Adeopapposaurus*; Am: *Amargatitanis*; Ap: *Apatosaurus*; Ba: "*Barosaurus africanus*"; Co: *Coloradisaurus*; Dc: *Dicraeosaurus*; Dp: *Diplodocus*; Gi: *Giraffatitan*; He: *Herrerasaurus*; La: *Lapparentosaurus*; Le: *Lessemsaurus*; Mu: *Mussaurus*; Pa: *Panphagia*; Pl: *Plateosaurus*; Ri: *Riojasaurus*; Ta: *Tazoudasaurus*; Vo: *Vouivria*. Thin-plate splines visualization of aligned theoretical right shapes along the first (B), second (C) and third (D) PC. Shape changes along each PC are represented for negative (left) and positive (right) extrema. They are represented, from left to right and top to down, in proximal, anterior, lateral, distal, posterior and medial views. In the proximal view, the top corresponds to the anterior side; to the posterior side in distal view, and to the proximal side in every other views. Anatomical abbreviations: asp: ascending process; ats: anterolateral triangular surface; das: distal articular surface; ds: distal swelling; las: lateral articular surface; lsf: lateral subfossa ma: medial apex; mba: medial border of the astragalus; mr: median ridge; msf: medial subfossa; pb: posterior bulge; pf: posterior fossa.

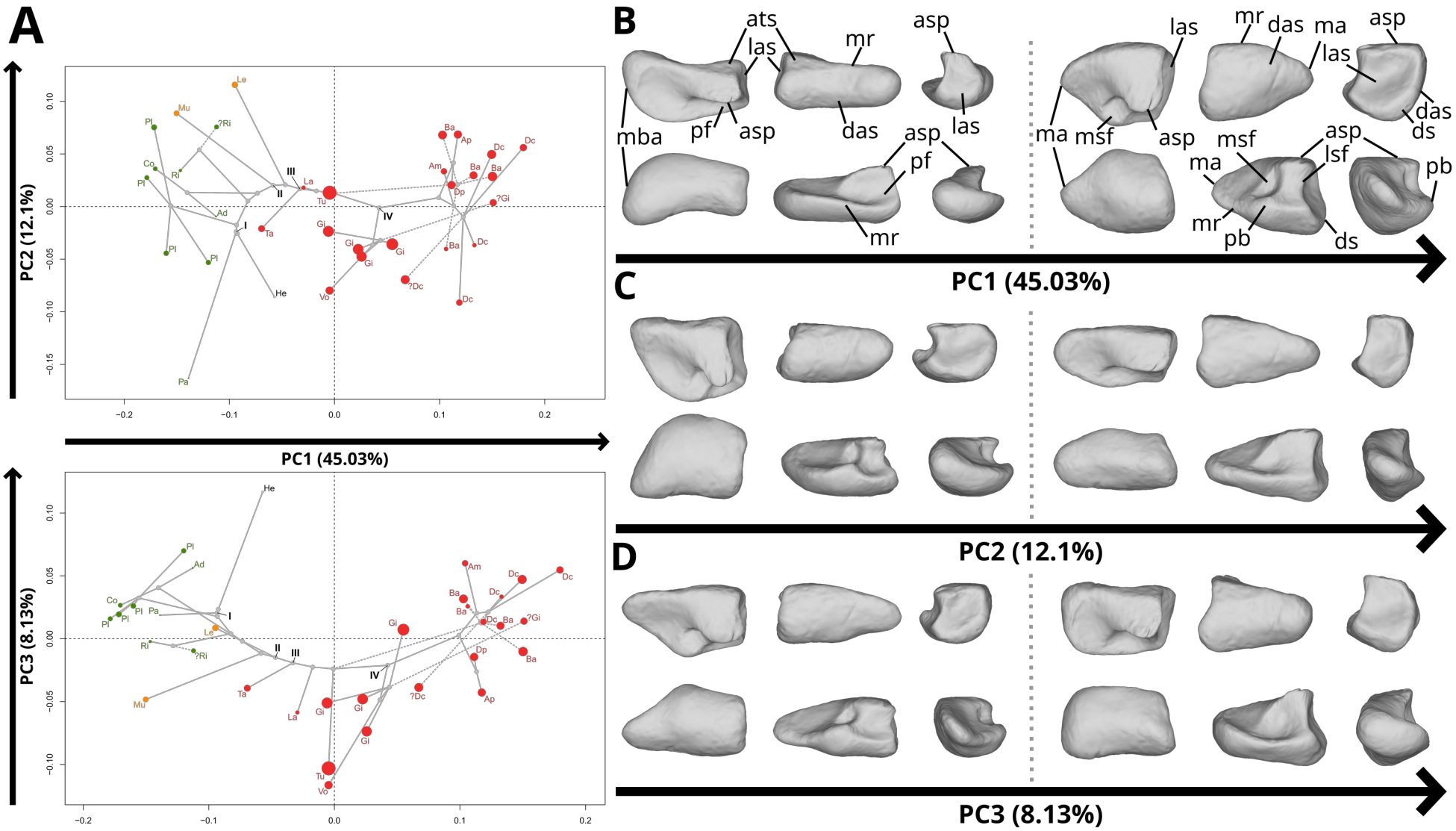
A
PC2 (12.1%)
PC1 (45.03%)
PC3 (8.13%)
B
ats
las
mr
asp
mba
pf
asp
das
asp
las
pf
mr
las
mr
das
ma
asp
las
das
ds
ma
msf
asp
msf
asp
ma
lsf
pb
mr
pb
ds
PC1 (45.03%)
C
PC2 (12.1%)
D
PC3 (8.13%)

Figure 5. Analysis of the common allometric component corrected for groups (columnarity or not). A, Bivariate plot of corrected CAC scores against the natural logarithm of the centroid size. Open circles: non-columnar taxa; filled circles: columnar taxa. Colours: Green: non-sauropodiform sauropodomorphs, orange: non-sauropodan sauropodiforms, red: sauropods, grey: outgroup (*Herrerasaurus*). B, Corresponding size-related variation: Shape changes at minimal size are shown in cyan, whereas shape changes at maximal size are shown in orange. Shape variation is represented, from left to right and top to down, in proximal, anterior, lateral, distal, posterior and medial views. In the proximal view, the top corresponds to the anterior side; to the posterior side in distal view, and to the proximal side in every other views. Anatomical abbreviations: asp: ascending process; ats: anterolateral triangular surface; das: distal articular surface; ds: distal swelling; las: lateral articular surface; lsf: lateral subfossa ma: medial apex; mba: medial border of the astragalus; mr: median ridge; msf: medial subfossa; pb: posterior bulge; pf: posterior fossa. Taxonomic abbreviations: Ad: *Adeopapposaurus*; Am: *Amargatitanis*; Ap: *Apatosaurus*; Ba: *"Barosaurus africanus"*; Co: *Coloradisaurus*; Dc: *Dicraeosaurus*; Dp: *Diplodocus*; Gi: *Giraffatitan*; He: *Herrerasaurus*; La: *Lapparentosaurus*; Le: *Lessemsaurus*; Mu: *Mussaurus*; Pa: *Panphagia*; Pl: *Plateosaurus*; Ri: *Riojasaurus*; Ta: *Tazoudasaurus*; Vo: *Vouivria*.

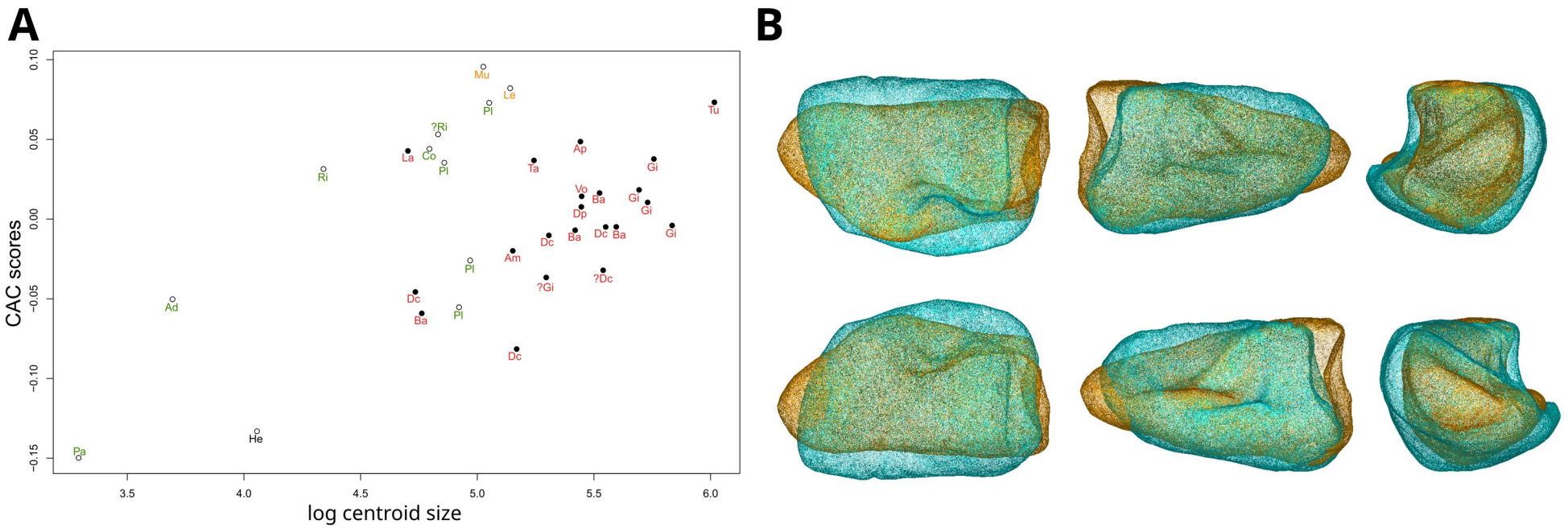
A
B
CAC scores
log centroid size
0.10
0.05
0.00
−0.05
−0.10
−0.15
3.5
4.0
4.5
5.0
5.5
6.0
Mu
Le
Pl
Tu
?Ri
La
Co
Pl
Ap
Ta
Gi
Ri
Vo
Ba
Gi
Gi
Dp
Dc
Ba
Dc
Ba
Gi
Am
Pl
?Dc
?Gi
Dc
Ad
Ba
Pl
Dc
Pa
He

Figure 6. Evolutionary rate estimation computed by the means of a phylogenetic ridge regression. A, Mapping of multivariate rates across sauropodomorph phylogeny using first (left; FAD) and last (right; LAD) possible occurrence dates of sampled taxa. Arabic numbers identify each internal node, while roman numbers highlight Sauropodomorpha (I), Sauropodiformes (II); Sauropoda (III); Neosauropoda (IV). B, Lollipop plots of estimated multivariate rates at each branch when using FAD (left) and LAD (right) topologies. In both plots, the red horizontal line corresponds to the median value, while the top and bottom dashed lines represent the upper and lower quartiles, respectively. Arabic and roman numbers correspond to labelling in A.

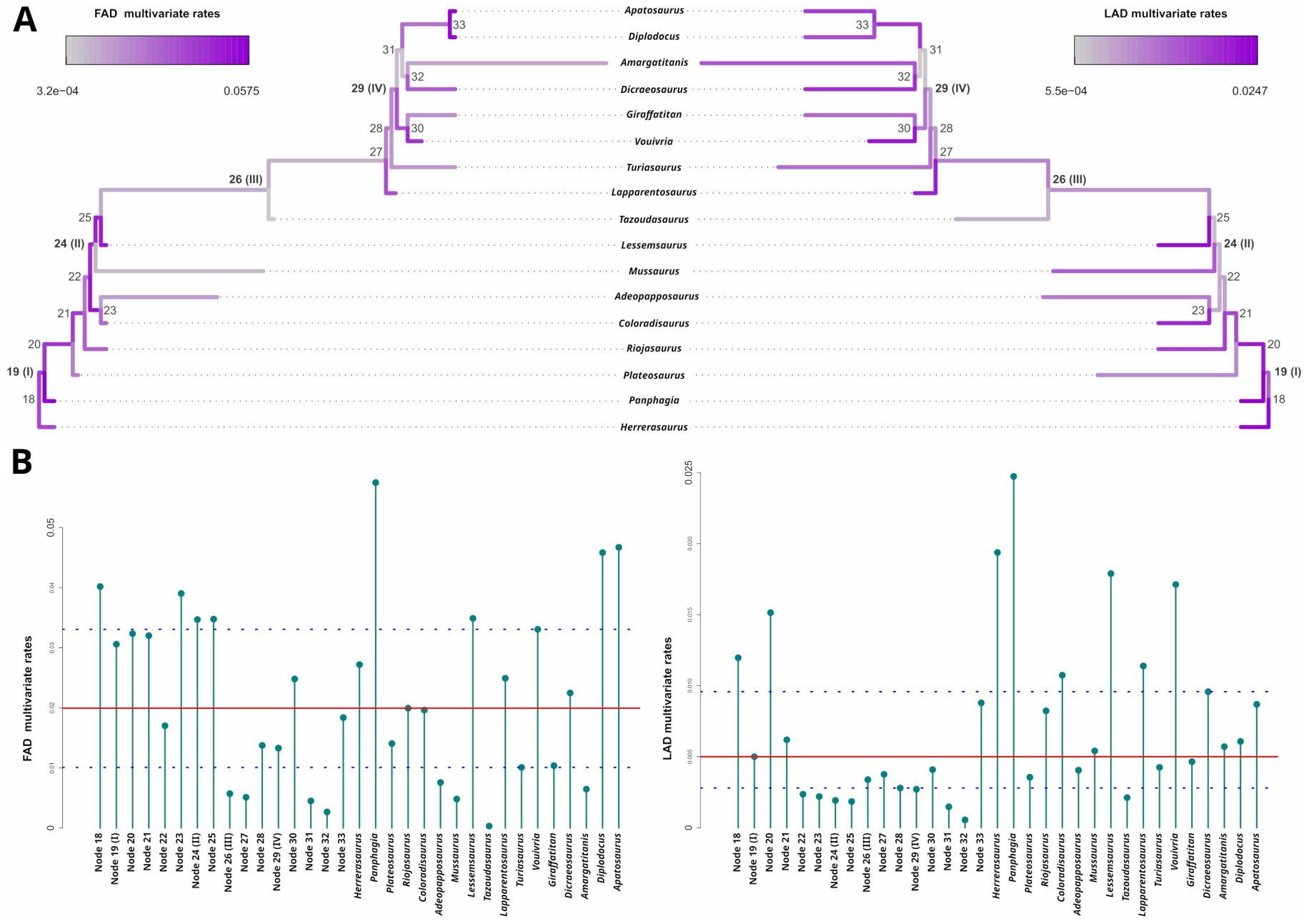
A
FAD multivariate rates
3.2e−04
0.0575
LAD multivariate rates
5.5e−04
0.0247
Apatosaurus
Diplodocus
Amargatitanis
Dicraeosaurus
Giraffatitan
Vouivria
Turiasaurus
Lapparentosaurus
Tazoudasaurus
Lessemsaurus
Mussaurus
Adeopapposaurus
Coloradisaurus
Riojasaurus
Plateosaurus
Panphagia
Herrerasaurus
19 (I)
24 (II)
26 (III)
29 (IV)
B
FAD multivariate rates
LAD multivariate rates
Node 18
Node 19 (I)
Node 20
Node 21
Node 22
Node 23
Node 24 (II)
Node 25
Node 26 (III)
Node 27
Node 28
Node 29 (IV)
Node 30
Node 31
Node 32
Node 33

Figure 7. Idealised astragalar morphotypes highlighted in this study, in anterolateral (top) and posteroproximal (bottom) views. Highlighted features indicated in Arabic numbers discriminate non sauropodan sauropodmorphs from (eu)sauropods, while those indicated in Roman numbers discriminate groups within sauropods. Features' states are detailed in Appendix S1 and in the discussion.

Morphotype A
Non-sauropodan sauropodomorphs

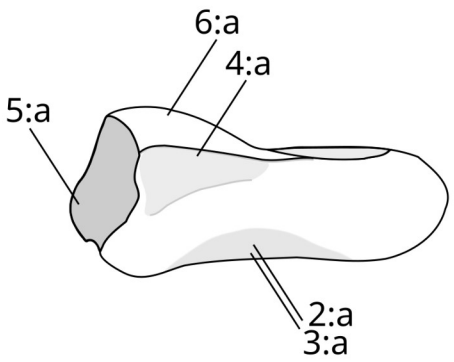

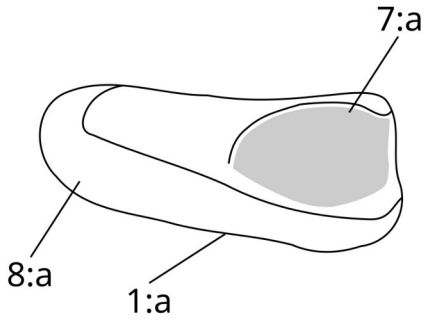

Morphotype B
Tazoudasaurus

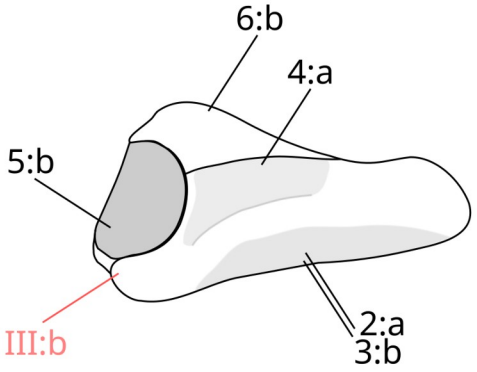

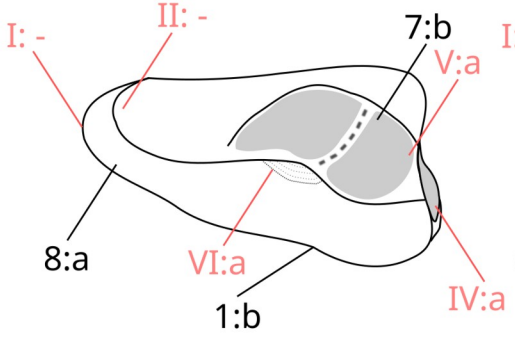

Morphotype C.1
Diplodocoidea (+"*Barosaurus africanus*")

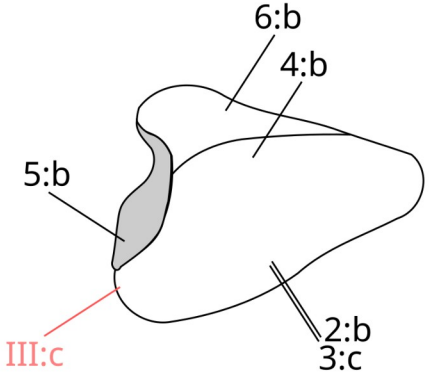

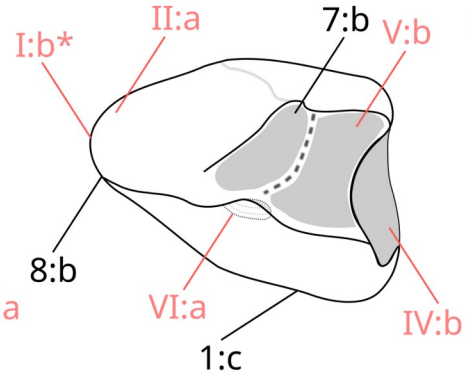

Morphotype C.2
Brachiosauridae (*a fortiori* Macronaria?)

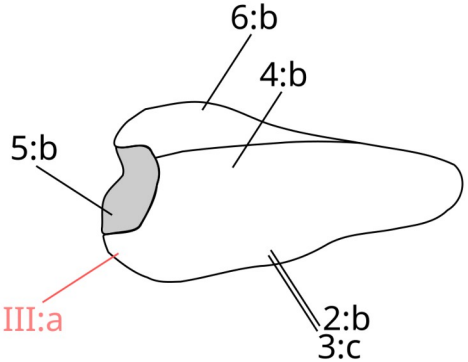

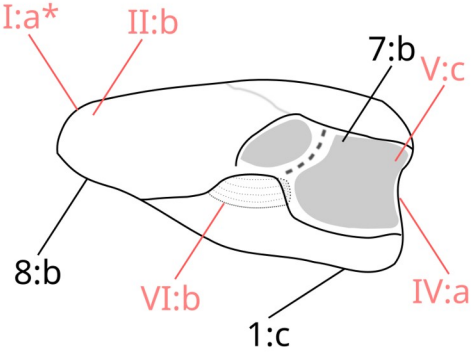

Tables

Table 1. Results of the analysis searching for significant shifts in evolutionary rates estimated by phylogenetic ridge regression. The significance was assessed for topologies with branch lengths arbitrarily set according to first (FAD) and last (LAD) appearance dates (ns: non significant p-value). The significance was also assessed for the sensitivity analysis accounting for stratigraphic uncertainty by randomization; the number of times significant shifts (towards lower and higher rates) were found out of the 1000 iterations and are indicated as percentages.

Node	FAD	LAD	randomized branch lengths (x1000)	
			Shifts to lower rates (%)	Shifts to higher rates (%)
27 (Lapparentosaurus + Turiasaurus + Neosauropoda)	ns	ns	51.4	0
28 (Turiasaurus + Neosauropoda)	ns	ns	47.5	0
29 (Neosauropoda)	ns	ns	19.1	0.1
31 (Diplodocoidea)	ns	ns	4.5	0.4

Table 2. Results of the sensitivity analysis searching for significant shifts in evolutionary rates estimated by phylogenetic ridge regression, when varying minimum branch length for internal nodes. The number of times significant shifts to lower (-) and higher (+) rates were found out of the 200 iterations and are indicated as percentages. Abbreviation: Mbl: minimum branch length.

Node	Mbl = 0.1 (x200)		Mbl = 0.5 (x200)		Mbl = 1 (x200)		Mbl = 2 (x200)		Mbl = 3 (x200)	
	- (%)	+ (%)	- (%)	+ (%)	- (%)	+ (%)	- (%)	+ (%)	- (%)	+ (%)
27	35.5	0.5	42.5	0	51.5	0	93.5	0	87	0
28	21	2.5	27	0	49.5	0	87	0	80	0
29	9	4	11	1.5	25.5	0	47.5	0	28	0
31	0.5	3.5	5.5	4.5	5.5	0.5	4.5	0	2	0

Table 3. Mean varibility in evolutionary rates estimated by phylogenetic ridge regression, expressed by coefficients of variation (CV_i = [standard $deviation_i$/$mean_i$]x100) calculated at a given node i. Abbreviations: Max: Maximum; Mbl: minimum branch length; Min: Minimum.

CV (%)	Mbl = 1 (x1000)	Mbl = 0.1 (x200)	Mbl = 0.5 (x200)	Mbl = 1 (x200)	Mbl = 2 (x200)	Mbl = 3 (x200)
Mean CV	42.1	78.28	57.38	41.93	27.09	22.31
Median CV	40	61.46	58.06	40.92	23.07	18.02
Min. CV	4.01	3.4	3.38	3.95	5.25	4.49
Max. CV	111.28	244.35	163.65	98.65	67.93	54.18

Supplementary Data

Figure S1. Morphospace resulting from the repeatability procedure.

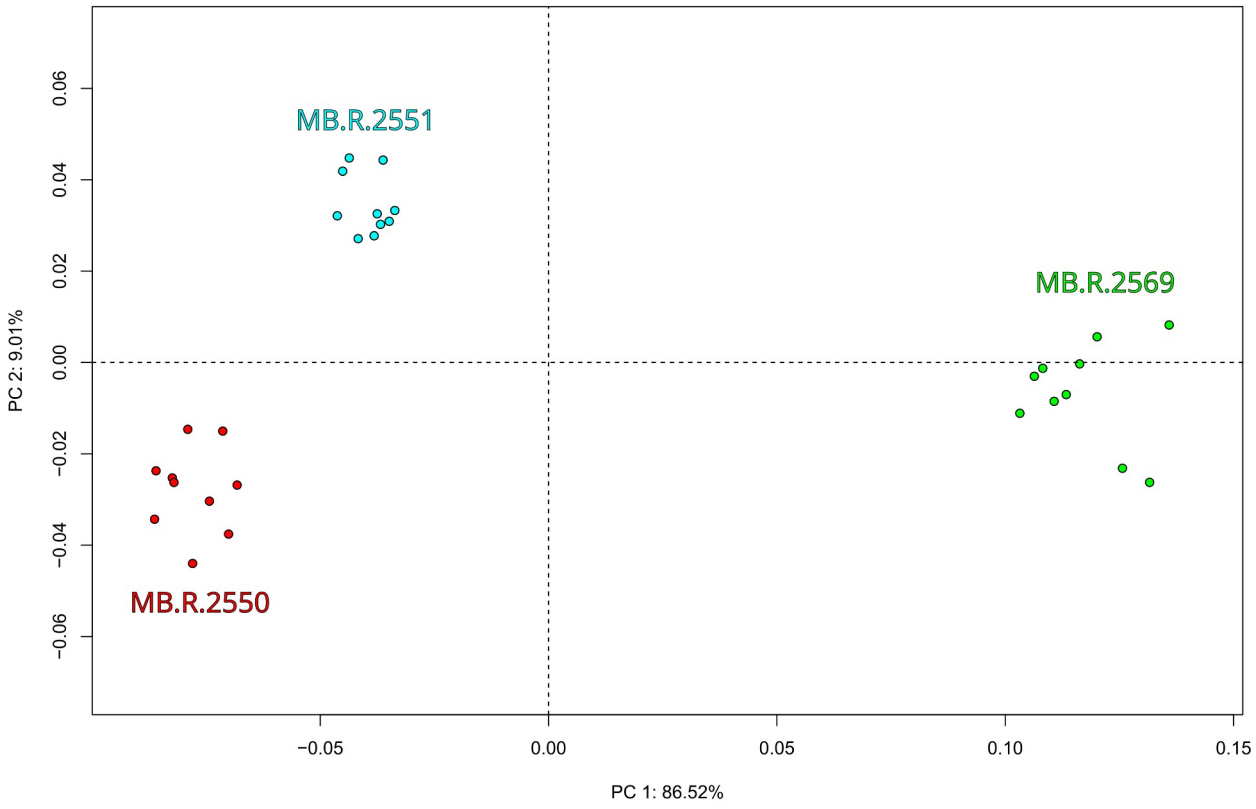

Figure S2. Morphospace showing the first and third PC for the analysis including titanosaurs. The diameter of the dots is proportional to specimens' centroid size. Colours: Green: non-sauropodiform sauropodomorphs, orange: non-sauropodan sauropodiforms, red: sauropods, grey: outgroup (*Herrerasaurus*), blue: indeterminate. Taxonomic abbreviations: Ad: *Adeopapposaurus*; Am: *Amargatitanis*; Ap: *Apatosaurus*; Ba: "*Barosaurus africanus*"; Bo: *Bonatitan*; Co: *Coloradisaurus*; Dc: *Dicraeosaurus*; Dp: *Diplodocus*; El: *Elaltitan*; Gi: *Giraffatitan*; He: *Herrerasaurus*; La: *Lapparentosaurus*; Le: *Lessemsaurus*; Mu: *Mussaurus*; Pa: *Panphagia*; Pl: *Plateosaurus*; Ri: *Riojasaurus*; Ta: *Tazoudasaurus*; Tv: *Tangvayosaurus*; Vo: *Vouivria*. The red convex hull represents space occupied by titanosaurs.

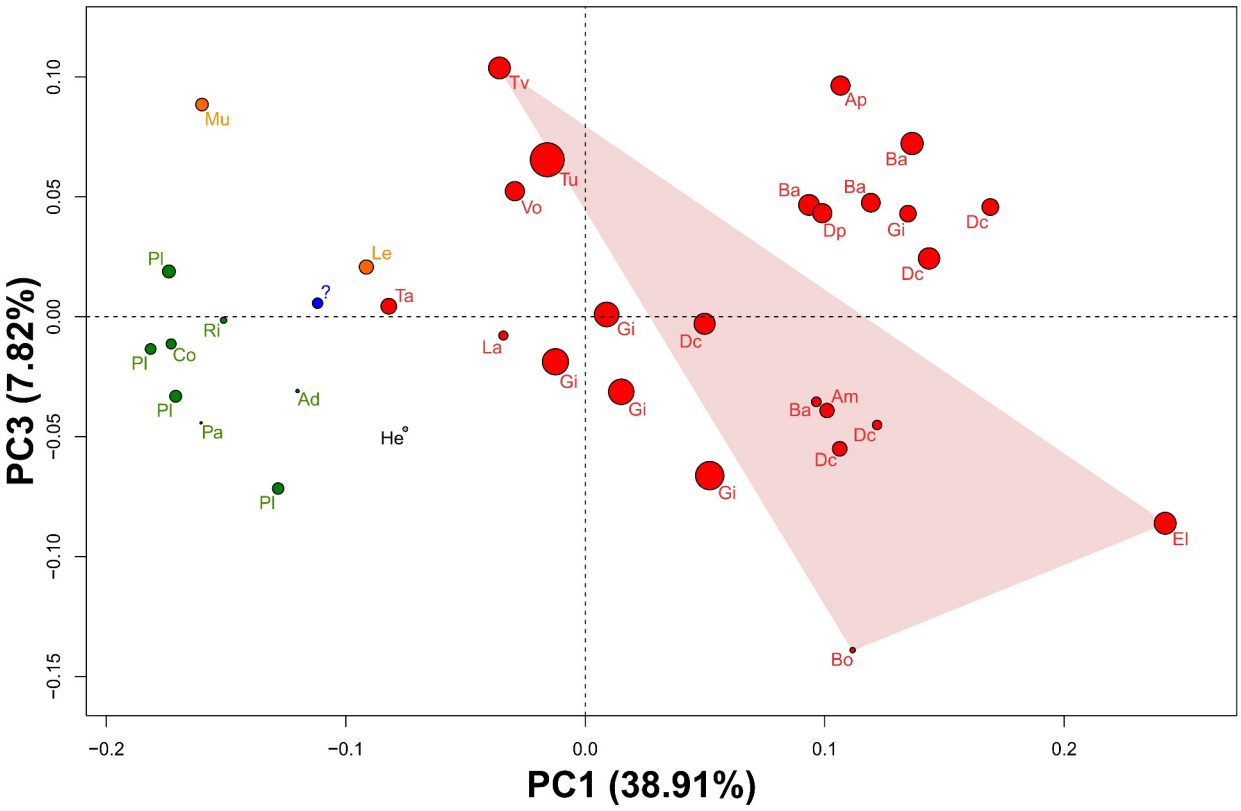

Table S1. Material sampled in this study

Institutional abbreviations: CPT, Museo de la Fundación Conjunto Paleontológico de Teruel-Dinópolis, Teruel, Spain; GPIT, Institute for Geosciences, Eberhard-Karls-Universität Tübingen, Tübingen, Germany; LFGT, Bureau of Land and Resources of Lufeng County, Lufeng, China; MACN, Museo Argentino de Ciencias Naturales Bernardino Rivadavia, Buenos Aires, Argentina; MB.R Museum für Naturkunde, Berlin, Germany; MDS, Musée des Dinosaures, Savannakhet, Laos; MF, Maison du Fossile, Lion-sur-Mer, France (definitively closed); MHNM Muséum d'Histoire naturelle, Marrakech, Morroco; MLP, Museo de La Plata, La Plata, Argentina; MNHN, Muséum National d'Histoire Naturelle, Paris, France; PVL, Instituto Miguel Lillo, Universidad Nacional de Tucumán, San Miguel de Tucumán, Argentina; PVSJ, Instituto y Museo de Ciencias Naturales, Universidad Nacional de San Juan, San Juan, Argentina; SMNS Staatliches Museum für Naturkunde, Stuttgart, Germany.

Other abbreviations:

Ori.: Orientation: Left (L) or Right (R)

Dig.: Digitization technique employed: CT-Scan (CT); P (P); SS (SS)

Cp: Qualitative evaluation of the completeness of the anatomical landmarks (Lk) and curves (Cu) locations: A: The incompleteness (if any) does not alter the placement of anatomical landmarks / the digitization of the curves; B: The incompleteness alters softly the placement of anatomical landmarks / the digitization of the curves; C: The incompleteness alters moderately the placement of anatomical landmarks / the digitization of the curves.

Taxonomic attribution	Collection number	Ori.	Dig.	Cp Lk	Cp Cu	Comments
Adeopapposaurus mognai	PVSJ 569	L	SS	A	B	Ascending process crest slightly damaged
Amargatitanis macni	MACN-PV-N53	R	SS	B	C	Anteromedial tip moderately damaged, fibular articular surface outline moderately blunt
Apatosaurus sp.	SMNS 10371	R	P	A	B	Ascending process crest moderately reconstructed
"Barosaurus africanus"	MB.R.2555	L	P	A	A	
"Barosaurus africanus"	MB.R.2563	L	P	A	A	Ascending process crest slightly reconstructed
"Barosaurus africanus"	MB.R.2566	L	P	B	C	Anteromedial tip slightly blunt; Ascending process crest slightly damaged; Distal border of the ridge of the fibular articular surface moderately blunt
"Barosaurus africanus"	MB.R.2567	L	P	B	B	Anteromedial tip slightly damaged; median ridge slightly blunt
Bonatitan reigi	MACN-RN-1061	L	SS	C	C	Interpretative landmarking following orientation in Salgado et al., 2015
Coloradisaurus brevis	PVL 5904	L	SS	A	A	Posterodistal border of the fibular articular surface possibly damaged
Dicraeosaurus hansemanni	MB.R.2569	R	P	B	B	Anteromedial tip slightly blunt; Distal border of the ridge of the fibular articular surface slightly blunt
Dicraeosaurus sattleri	MB.R.2550	R	P	A	A	Ascending process crest substantially reconstructed
Dicraeosaurus sattleri	MB.R.2551	L	P	A	A	Ridge of the fibular articular surface slightly damaged; Ascending process crest moderately reconstructed
Dicraeosaurus sattleri	MB.R.2554	L	P	B	C	Ascending process crest moderately broken; median ridge slightly

						broken anteriorly
Dicraeosaurus sp. (?)	MB.R.2557	L	P	A	A	taxonomic attribution questioned regarding our results
Diplodocus sp.	GPIT-PV-31370	R	CT	A	A	
Elaltitan lilloi	PVL 4628	R	SS	B	C	Anteromedial tip moderately damaged; Anterior border of the median ridge poorly preserved. Orientation following Mannion & Otero (2012).
Giraffatitan brancai (?)	MB.R.2559	L	P	A	B	Ascending process crest slightly damaged; taxonomic attribution questioned regarding our results
Giraffatitan brancai	MB.R.2561	R	P	B	B	Distal border of the ridge of the fibular articular surface moderately damaged; Ascending process crest slightly damaged (a small portion is also slightly reconstructed)
Giraffatitan brancai	MB.R.2562	L	P	A	B	Ascending process crest slightly damaged ; distal border of the fibular articulating surface ridge slightly damaged
Giraffatitan brancai	MB.R.2568	R	P	A	A	
Giraffatitan brancai	MB.R.2570	L	P	B	C	Poor preservation of the ridge of the fibular articular surface; Ascending process crest slightly damaged
Herrerasaurus ischigualastensis	PVSJ 373	L	SS	A	A	
Lapparentosaurus madagascariensis	MNHN.F.MAA132	R	P	A	A	Ascending process crest possibly blunt
Lessemsaurus sauropoides	PVL 4822-58	L	SS	C	C	Anteromedial tip slightly blunt; Distal border of the ridge of the fibular articular surface damaged
Mussaurus patagonicus	MLP 68-II-27-1	R	SS	B	C	Anteromedial tip moderately blunt; surface quite poorly preserved

Panphagia protos	PVSJ 874	R	P	B	C	Ascending process crest moderately broken
Plateosaurus trossingensis	GPIT RE7288 (I)	R	CT	A	A	
Plateosaurus trossingensis	SMNS 13200 #1	L	P	A	A	Neotypic specimen
Plateosaurus trossingensis	SMNS 13200 #2	R	P	A	A	Anteromedial tip slightly blunt; specimen different from the neotype but with the same collection number
Plateosaurus trossingensis	SMNS 91296 (F10)	R	P	A	A	
Riojasaurus incertus	PVL 3663	R	SS	A	B	Ascending process crest slightly damaged
Sauropodomorpha indet.	PVL 3855	L	SS	B	B	See results for tentative taxonomic attribution (only for phylomorphospace analysis); slight damages on the fibular facet and the posterior side of the medial outline
Tangvayosaurus hoffeti	MDS TV2	L	P	A	A	
Tazoudasaurus naimi	MHNM To1-31 (cast)	R	SS	A	B	Anterior border of the median ridge slightly blunt
Turiasaurus riodevensis	CPT-1244 (cast)	R	P	B	C	moderate alteration of the fibular and ascending process articulating surfaces
Vouivria damparisiensis	MNHN.F.1934.6 DAM 11	L	P	A	A	

Other specimens examined but not included due to critical incompleteness and/or deformations:

Taxon (original attribution)	Collection number
Amargasaurus cazui	MACN-PV-N15
“Barosaurus africanus”	MB.R.2560
Bonatitan reigi	MACN-RN-821
“Calvadosaurus dubrulli”	MF MDV 8 (cast)
Giraffatitan brancai	MB.R.2553
Giraffatitan brancai	MB.R.2556
Mussaurus patagonicus	MLP 61-III-20-22
Xingxiulong chengi	LFGT-D0003

Table S2. Landmark set used in this study.

Landmark #	Anatomical definition (mainly following the terminology used in Allain & Aquesbi, 2008)
1	Intersection point between the crest posteriorly bordering the ascending process and the ridge outlining the lateral articular surface
2	Intersection point between the margin of the ridge outlining the lateral articular surface and the most anteroproximal branch of the median ridge delimiting the proximal and distal faces *
3	Intersection point between the margin of the ridge outlining the lateral articular surface and the posterior border of the median ridge delimiting proximal and distal faces
4	Medialmost point of the median ridge delimiting proximal and distal faces
5	Termination of the crest posteriorly bordering the ascending process, separating the medial tibial articular surface and the posterior fossa

*Note about homology hypotheses: anteroproximally, most non-sauropodan sauropodomorph specimens show two ridges connecting with the lateral articular surface outline, whereas there is only one ridge in sauropods. The most proximal one is inferred here as homologous to the only ridge seen in sauropods, based connection principle, as in both forms it defines the anterior border of the articular surface with the tibial descending process.

Curve #	Anatomical definition	Number of semilandmarks
1	Ridge connecting landmarks #1 & #2	10
2	Ridge connecting landmarks #2 & #3	20
3	Ridge connecting landmarks #3 & #1	10
4	Ridge connecting landmarks #3 & #4	30
5	Ridge connecting landmarks #4 & #2	30
6	Ridge connecting landmarks #1 & #5	20

	Anatomical landmarks	Curve sliding semilandmarks	Surface sliding semilandmarks	Total
Number of landmarks used in this study	5	120	678	803

Landmark disposition on the template (*Tazoudasaurus*). Labelled red dots denote anatomical landmarks; blue dots correspond to curve sliding semilandmarks, and green dots to surface sliding semilandmarks.

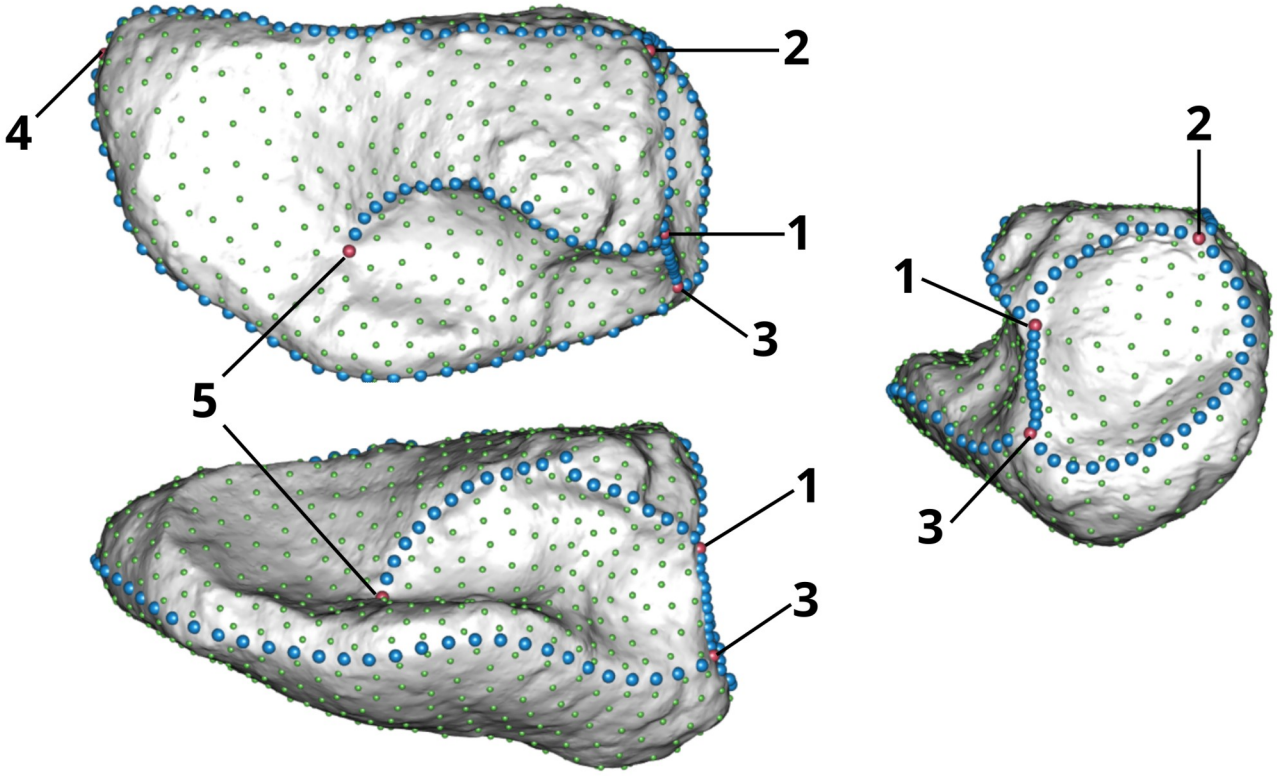

Table S3. Results of the Procrustes ANOVA testing for effect of size, columnarity and their interaction on shape (aligned landmark coordinates). Significant effects ($p < 0.05$) in bold.

-- When size is incorporated first in the linear model

Factor	R^2	Z	P-value
log(centroid size)	0.15042	3.2012	**0.0002**
columnarity	0.24943	3.7556	**1e-04**
interaction	0.02845	1.1155	0.1348

-- When columnarity is incorporated first in the linear model

Factor	R^2	Z	P-value
columnarity	0.35300	3.6758	**1e-04**
log(centroid size)	0.04685	2.1853	**0.0142**
interaction	0.02845	1.1155	0.1348

Appendix S1 A, Summary of the morphological features characterizing the morphotypes described in discussion (section 1) and in Fig. 7; B, Summary of the morphological features characterizing the morphotypes described in discussion (section 2) and in Fig. 7.

Appendix S1 (A): Summary of the morphological features characterizing the morphotypes described in discussion (section 1) and in Fig. 7

Feature	State in morphotype			Existing related character(s)?
	A	B	C	
1 – General shape	rectangular and mediolaterally elongated (a)	intermediate (b; see text)	wedge-shaped (c)	Yes
2 – Distal articular surface shape	saddle-shaped (centrally concave) (a)	saddle-shaped (centrally concave) (a)	smoothly convex distal roller (b)	Yes
3 – Distal articular surface orientation	Poorly anterodistally oriented (a)	Moderately anterodistally oriented (b)	strongly anterodistally oriented (c)	No (but see text)
4 – Anterolateral triangular surface	present (a)	present (a)	absent (b)	Partly
5 – Lateral articular surface	trilobate, flat and with no outlining ridge (a)	subcircular to subpentagonal, concave and with an outlining ridge (b)	subcircular to subpentagonal, concave and with an outlining ridge (b)	No
6 – Ascending process	strongly bevelled, more developed mediolaterally (a)	less bevelled, more developped anteroposteriorly (b)	less bevelled, more developped anteroposteriorly (b)	Yes
7 – Crest separating the posterior fossa into two subfossae	absent (a)	present (b)	present (b)	Yes
8 – Medial half	developed, squared and distally thick (a)	developed, squared and distally thick (a)	reduced to a triangular and distally thin apex (b)	Partly

1452 **(B): Summary of the morphological features characterizing the morphotypes described in discussion (section 2) and in Fig. 7.**

Feature	State in morphotype					Existing related character(s)?
	B	C.1	C.2	*Lapparentosaurus*	*Turiasaurus*	
I – Medial apex development (* = likely size-related)	-	Usually very poorly developed medially (b*)	Usually fairly developed medially (a*)	Fairly developed medially (a)	Fairly developed medially (a)	Yes
II – Medial apex deflection	-	not deflected (a)	anteromedially deflected (b)	not deflected (a)	not deflected (a)	No
III – Lateral swelling	Intermediately developed (b)	strongly developed (c)	poorly developed (a)	poorly developed (a)	poorly developed (a)?	Yes
IV – Lateral articular surface	laterally oriented (a)	posterolaterally oriented (b)	laterally oriented (a)	laterally oriented (a)	laterally oriented (a)	Yes
V – Posterior subfossae	medial subfossa is much larger than the lateral one (a)	both subfossae are subequal in size (b; see also text)	lateral fossa is much larger than the medial one (c)	lateral fossa is much larger than the medial one (c)	lateral fossa is much larger than the medial one (c)	No
VI – Posterior bulge	modestly developed (a)	modestly developed (a)	Strongly developed (b)	modestly developed (a)	strongly developed (b)	Partly

Supplementary Data 1. Correspondence between absolute ages and stratigraphic ranges based on Otero & Peyre de Fabrègues, 2021 and Royo-Torres et al. 2017.

Taxon	FAD	LAD	Reference
Herrerasaurus	231.4	228.91	Langer et al. 2022
Panphagia	231.4	228.91	Langer et al. 2022
Plateosaurus trossingensis	227	201.3	Otero & Peyre de Fabrègues,2022
Riojasaurus	221.8	213	Otero & Peyre de Fabrègues,2022
Coloradisaurus	221.8	213	Otero & Peyre de Fabrègues,2022
Adeopapposaurus	201.3	190.8	Otero & Peyre de Fabrègues,2022
Mussaurus	192.78	192.74	Pol et al. 2021
Lessemsaurus	221.8	213	Otero & Peyre de Fabrègues,2022
Tazoudasaurus	190.8	174	Allain & Aquesbi, 2008
Lapparentosaurus	168.3	166.1	Royo-Torres et al., 2017
Turiasaurus	157.3	139.8	Royo-Torres et al., 2017
« Barosaurus africanus »	157.3	145	Remes, 2009
Dicraeosaurus	157.3	145	Remes, 2009
Amargatitanis	129.4	125	Gallina et al., 2022
Diplodocus	157.3	145	Tschopp et al., 2015
Apatosaurus	157.3	145	Tschopp et al., 2015
Vouivria	163.5	157.3	Mannion et al., 2017
Giraffatitan	157.3	145	Remes, 2009
Tangvayosaurus	125	100.5	Allain et al., 1999
Elaltitan	96	88.5	Lamanna et al. 2002 ; Mannion & Otero, 2012
Bonatitan	83.6	66	Salgado et al., 2014

Correspondence between absolute ages and stratigraphic ranges based on Otero & Peyre de Fabrègues, 2021 and Royo-Torres et al., 2017

Supplementary Data 2a. Description of shape deformation along PC extrema in the first PCA (Analysis 1) including all specimens; **2b.** Description of shape deformation along the second PC extrema of the phylomorphospace analysis (Analysis2, Fig. 4C).

Supplementary Data 2a. Description of shape deformation along PC extrema in the first PCA (Analysis 1) including all specimens.

PC1 accounts for 38.91% of the total variation (Fig. 2B). The distribution of taxa is similar to what was described in the phylomorphospace analysis (see results, Fig.4), but with *Elaltitan* plotting at the positive extremity. Shape variations are similar for the negative extremity compared to the phylomorphospace analysis; the shape of the positive extremity is also globally similar, being slightly more expanded anteroposteriorly, with an even more reduced medial area and a sharper medial apex. The lateral half of the shape is more developed proximodistally and less laterally.

PC2 accounts for 18.47% of the total variation (Fig 2B). Variation along this axis is strongly dominated by titanosaurs specimens, with *Tangvayosaurus* alone at the negative extremity and *Elaltitan* alone at the positive one. *Bonatitan* is plotting as with the second most negative value, quite far from *Tangvayosaurus*, and far from all other taxa. The shape at negative extremity appears as much more projecting proximally and being extremely flattened anteroposteriorly. The shape at the positive extremity appears as much more projecting posteriorly and being much more flattened proximodistally.

PC3 accounts for 7.82% of the total variation (Fig S2). Variation along this axis is dominated by titanosaurs, with *Bonatitan* alone at the negative extremity and several taxa at the positive one. *Tangvayosaurus* has the most positive value along this axis, while *Elaltitan* has the second most negative one.

The shape at negative extremity appears more developed posteriorly and less anteriorly and mediolaterally than in its equivalent in the phylomorphospace analysis (Fig. 4D, shape at the positive extremity), and also differs by having distinguished medial and lateral subfossae, the former being more anteriorly placed and slightly more concave than the latter. The shape at positive extremity appears more developed anteriorly, medioposteriorly and laterally and less posteriorly than in its equivalent in the phylomorphospace analysis (Fig. 4D, shape at the negative extremity), and also differs by having a more posteriorly placed and barely distinguishable medial subfossa.

Supplementary Data 2b. Description of shape deformation along the second PC extrema of the phylomorphospace analysis (Analysis2, Fig. 4C).

General outline: The shape at the negative extremity has a subsquare general outline in proximal view, all borders being roughly equally developed. All corners are roughly square-angled except the posteromedial one, being reduced to a gentle convexity. In anterior view, the distal outline is not bevelled, but might be interpreted as such if slightly rotated anteriorwards (see discussion part 1.1) The shape at the positive extremity is elongated mediolaterally in proximal view. Its medial border is rounded and slightly less developed, and the middle of the posterior border is smoothly convex. The shape of the positive extremity is wedge-shaped *sensu* Wilson & Sereno (1998) in posterior view.

Distal surface: The general distal curvature of the negative shape is only subtly varying, being smoothly convex with a subtle concavity along the mediolateral axis in its anteriormost part. The distinction between the posterior and anterior parts of this region is barely discernible. The posterior part is distally oriented and extended posteriorly, and the anterior part is anteriorly oriented and regularly convex. The general distal curvature of the positive shape is sharply varying, being irregularly convex with an acute bulge delimiting its posterior and anterior parts. The posterior part is posterodistally oriented and reduced, and the anterior part is anteriorly oriented and is almost flat.

Lateral surface: The lateral articular surface is, in the negative shape, oriented laterally so that it is not visible in posterior view. In lateral view, the lateral articular surface is concave and developed anteroposteriorly. Its outline is marked by a low anterodistal bulge more swollen laterally. In the positive shape, the lateral articular surface is slightly more posterolaterally oriented and partly visible. In lateral view, the lateral articular surface is concave narrower anteroposteriorly, but showing an anteroproximal projection. Its outline is marked by a low distal bulge more swollen laterally.

Proximolateral surface (Ascending process and posterior fossa(e)): In the negative shape, the ascending process is poorly developed along the mediolateral axis in proximal view, but its lateralmost part is extensively developed along the anteroposterior axis. The posterior crest is sigmoidal, with its lateral part being convex posteriorly and its medial part, joining the main body, being concave. Anteriorly, the lateralmost part of the median ridge delimits the ascending process and the distal surface by a tiny blunt surface. The fossa posterior to the ascending process is split in two subfossae by a crest extending to the posterior side of the median ridge. The junction between this crest and the median ridge is marked by a bulge. The medial subfossa is smaller and elliptic and more shifted centrally. The lateral subfossa is larger and hourglass-shaped, with its proximal border shorter than the distal one. Both subfossae are deeply concave and sharply delimited.

In the positive shape, the ascending process is extensively developed along the mediolateral axis, in proximal view, but also fairly developed along the anteroposterior axis. The posterior crest is in its lateral part monotonously horizontal in its lateral part and is progressively deflecting posteromedially in its medial part connecting with the main body. Anteriorly, the ascending process directly contacts the distal articular surface. The posterior border of the ascending process is marked by a large fossa, delimited medially from the rest of the main body by a low ridge (*i.e.* the medial part of the posterior crest), and laterally from the lateral articular surface by a ridge. The posterior fossa is globally flatter, but occupying a larger area. Its medial part is relatively deeper than the lateral one.

Proximomedial articular surface: In the negative shape, the medial part of the main body decreases in extension posteriorly. Its proximal surface is smoothly concave, while its anteromedial tip (*i.e.*, the medial part of the median ridge) is proximodistally thick. In the positive shape, the medial part of the main body is elongated mediolaterally. Its proximal surface is more concave, with a noticeably steeper transition with the proximal surface of the ascending process. The rounded medial extremity is thin proximodistally.